

MINISTRY OF EDUCATION



**THE ANNALS OF
“DUNAREA DE JOS”
UNIVERSITY OF GALATI**

Fascicle IX
METALLURGY AND MATERIALS SCIENCE

YEAR XLI (XLVI)
September 2023, no. 3

ISSN 2668-4748; e-ISSN 2668-4756



2023
GALATI UNIVERSITY PRESS

EDITORIAL BOARD

EDITOR-IN-CHIEF

Assist. Prof. Marius BODOR – “Dunarea de Jos” University of Galati, Romania

SCIENTIFIC ADVISORY COMMITTEE

Assist. Prof. Dragos-Cristian ACHITEI – “Gheorghe Asachi” Technical University Iasi, Romania

Assoc. Prof. Stefan BALTA – “Dunarea de Jos” University of Galati, Romania

Assist. Prof. Chenna Rao BORRA – Indian Institute of Technology, Republic of India

Prof. Acad. Ion BOSTAN – Technical University of Moldova, the Republic of Moldova

Researcher Mihai BOTAN – The National Institute of Aerospace Research, Romania

Prof. Vasile BRATU – Valahia University of Targoviste, Romania

Prof. Francisco Manuel BRAZ FERNANDES – New University of Lisbon Caparica, Portugal

Prof. Bart Van der BRUGGEN – Katholieke Universiteit Leuven, Belgium

Prof. Acad. Valeriu CANTSER – Academy of the Republic of Moldova

Prof. Valeriu DULGHERU – Technical University of Moldova, the Republic of Moldova

Prof. Gheorghe GURAU – “Dunarea de Jos” University of Galati, Romania

Assist. Prof. Gina Genoveva ISTRATE – “Dunarea de Jos” University of Galati, Romania

Postdoc. Researcher Nora JULLOK – University of Oulu, Finland

Prof. Rodrigo MARTINS – NOVA University of Lisbon, Portugal

Prof. Strul MOISA – Ben Gurion University of the Negev, Israel

Assist. Prof. Priyanka MONDAL – CSIR-Central Glass and Ceramic Research Institute, India

Prof. Daniel MUNTEANU – “Transilvania” University of Brasov, Romania

Assoc. Prof. Alina MURESAN – “Dunarea de Jos” University of Galati, Romania

Prof. Maria NICOLAE – Politehnica University Bucuresti, Romania

Assist. Prof. Manuela-Cristina PERJU – “Gheorghe Asachi” Technical University Iasi, Romania

Prof. Cristian PREDESCU – Politehnica University of Bucuresti, Romania

Prof. Iulian RIPOSAN – Politehnica University of Bucuresti, Romania

Prof. Antonio de SAJA – University of Valladolid, Spain

Assist. Prof. Rafael M. SANTOS – University of Guelph, Canada

Prof. Ion SANDU – “Al. I. Cuza” University of Iasi, Romania

Prof. Mircea Horia TIHEREAN – “Transilvania” University of Brasov, Romania

Prof. Ioan VIDA-SIMITI – Technical University of Cluj Napoca, Romania

Assoc. Prof. Petrica VIZUREANU – “Gheorghe Asachi” Technical University Iasi, Romania

EDITING SECRETARY

Assist. Prof. Marius BODOR – “Dunarea de Jos” University of Galati, Romania

Assist. Nicoleta BOGATU – “Dunarea de Jos” University of Galati, Romania

Assist. Prof. Eliza DANAILA – “Dunarea de Jos” University of Galati, Romania

Assist. Prof. Florin Bogdan MARIN – “Dunarea de Jos” University of Galati, Romania

Assist. Prof. Mihaela MARIN – “Dunarea de Jos” University of Galati, Romania



Table of Contents

1. Nicolae Tiberiu CIOBANU, Adriana Gabriela ŞCHIOPU - Hydrogen Production and Solid-State Storage: A Review	5
2. Adrian LEOPA - Regarding the Use of Finite Element Modeling for Propulsion System Sizing in V.T.O.L. Drones	15
3. Doina BOAZU - Determination of Stress Concentration Factor for a Rectangular Bar with Fillet Under Axial Loading: An Artificial Neural Networks Approach	20
4. Doina BOAZU - Determination of Stress Concentration Factor for a Stepped Bar Under Bending Loading: An Artificial Neural Networks Approach	29
5. Simona STANCA - Challenges in Integrating Green Buildings into Everyday Life	39
6. Silvia-Iuliana NECULA, Vasile BAŞLIU, Vasile BRIA, Marius BODOR - Comparative Study Regarding the Design of a 3D Printed Hip Prosthesis	46
7. Carmelia Mariana BĂLĂNICĂ DRAGOMIR - Recovery of Agricultural Waste to Obtain Compost	54



THE ANNALS OF "DUNAREA DE JOS" UNIVERSITY OF GALATI
FASCICLE IX. METALLURGY AND MATERIALS SCIENCE
Nº. 3 - 2023, ISSN 2668-4748; e-ISSN 2668-4756
Volume DOI: <https://doi.org/10.35219/mms.2023.3>

HYDROGEN PRODUCTION AND SOLID-STATE STORAGE: A REVIEW

Nicolae Tiberiu CIOBANU¹, Adriana Gabriela ŞCHIOPU²

¹Institute for Nuclear Research Pitesti, 1 Campului Street, 115400 Mioveni, Romania

²Department of Materials Engineering, University of Pitesti, no. 1 Târgul din Vale street, Pitesti, Romania
e-mail: plaiasugabriela@yahoo.fr

ABSTRACT

This paper is a synthesis of the methods used for hydrogen production and the storage of hydrogen in the form of metal hydrides and different methods of hydrogen storage in various materials are presented. It also presents the Romanian vision in relation to the existing and future projects that include the production of hydrogen and its use in energy.

KEYWORDS: hydrogen production, hydrogen storage materials, metal hydrides

1. Introduction

1.1. General information about hydrogen

Hydrogen, with the symbol H and atomic number 1, has an atomic weight of 1.008, is the lightest element in the periodic table of elements. In monatomic form, it is the most widespread element in the universe, being found in a proportion of 75%. The most common isotope of hydrogen is protium (having the symbol ¹H), which is composed of a proton and devoid of neutrons [1].

Table 1. Physico-chemical properties of hydrogen [1]

Phase at STP*	Gas
Density	0.08988 g/L (0 °C, 1 bar)
Melting point	-259.14 °C
Boiling point	-252.87 °C
Molar heat capacity	(H ²) 28,836 j.mol ⁻¹ K ⁻¹
Ionization potential	13.5984 eV
Specific heat	14,304 j/gK
Crystal structure	Hexagonal
Thermal conductivity	0.1805 Wm ⁻¹ .k ⁻¹

*Standard temperature and pressure

In nature, the most stable and common isotopes of hydrogen are:

1. Protium (0 neutrons, atomic number A = 1);

2. Deuterium (1 Neutron, atomic number A = 2);
3. Tritium (2 neutrons, atomic number A = 3).

1.2. Use of hydrogen

Hydrogen is one of the most viable energy sources for the future. It has a large energy storage capacity, and does not pollute if it is used as a fuel for transport, heating and electricity generation, in geographical areas where it is difficult to implement the infrastructure for electricity use [1].

Globally, this chemical element is considered to be the second source of energy, as an energy carrier. The energy carrier is used to transport, store and deliver energy in a form that is easy to use. Also, hydrogen is a contender for the future, in terms of energy, because a large volume of hydrogen can be easily stored in various forms. It is considered to be very efficient; its degree of pollution tends to zero and there is the possibility of being used in the field of transport, heat generation and electricity production [1].

2. Hydrogen production

Hydrogen can be obtained by the following methods:

1. extraction from hydrocarbons;
2. production from coal;
3. thermo-chemical processing of biomass;
4. electrolysis of water.

Through steam reforming, hydrogen will be extracted from hydrocarbons (natural gas) in two phases [2].

By adding steam at a temperature of around 500-800 °C and a pressure of 20-40 bar, the more complex hydrocarbons are broken down into methane, hydrogen, carbon monoxide as well as carbon dioxide to avoid clogging the catalyst in the reformer assembly. Methane will then react with the water in the presence of a nickel catalyst at a temperature of 700-1100 °C and a pressure of 25-30 bar, resulting in H₂ and CO [2].

The negative side of this process is that the secondary products, CO₂, CO and other gases, because if are released into the atmosphere, it will have a strong greenhouse effect [2].

Biomass comprises of hydrocarbons and other waste streams, such as wastewater, which also contain organic substances from which hydrogen can be extracted. Hydrogen can be obtained from biomass by catalytic reforming with steam. Due to the fact that biomass contains up to 40% oxygen, it gasifies almost by itself [3].

There are different methods to produce hydrogen from water, such as: electrolysis of water, high-pressure electrolysis, high-temperature electrolysis, biocatalyzed electrolysis, radiolysis, thermolysis, and reaction with ferrosilicon [4]. A new method, developed in 2017 by researchers from the U.S. Army, can produce hydrogen by the interaction between water and powder based on nanogalvanic aluminium [5].

By the end of 2021, the origin of hydrogen production globally is: 47% natural gas, 27% coal, 22% petroleum, and 4% water electrolysis [6].

In Europe, hydrogen is currently used in less than 2% of energy consumption and is mostly used for the manufacturing of chemical products. A percentage of 96% of the hydrogen produced using natural gas, negatively affects the environment by producing significant amounts of CO₂ emissions [7].

In 2022, in Romania, steps were started to build several electrolysis plants, with a capacity of at least 100 MW each, which will be able to produce up to 10,000 tons of hydrogen, starting in 2025. The fields in the country that can use hydrogen as energy are industry, transport, district heating, but also energy storage after 2030 [8].

3. Hydrogen storage

Hydrogen can be stored in several ways, such as:

1. hydrogen as gas;
2. hydrogen storage in liquid form;
3. hydrogen storage in solid form.

3.1. Storage as gas in pressure vessels

One kilogram of hydrogen occupies a volume of 11 m³ at normal pressure and temperature, and usually this type of storage requires high compression. Storing H₂ in gas form requires pressured vessels that withstand pressures between 3.5*10⁶ and 7*10⁶ Pa. High-strength steels or other metals are an option for hydrogen storage pressure vessels, but the diffusivity of hydrogen in the metal and the weight of the metal must also be considered. Other variants for the metals that can be used for the manufacturing of hydrogen pressure vessels are austenitic steels, but their high weight makes them impossible to be used for this purpose [9].

3.2. Storage of hydrogen in liquid form

The energy density of hydrogen can be doubled compared to 68947.57 kPa of CH₂ for 70 g/L, by liquefaction at a temperature of 20 K, at atmospheric pressure. Five kg of hydrogen occupies a volume of only 71 L, which is equal to the volume currently occupied by the fossil fuel used in motor vehicles. The hydrogen phase diagram illustrates the appearance of different forms of hydrogen depending on temperature and pressure. There is a narrow segment where hydrogen can be found in liquid form with a density of 70.8 kg/m³, at a temperature of 20 K [9].

The energy required to obtain liquid H₂ represents approximately 30% of the lowest heating value of hydrogen. For these systems, there is a period when the hydrogen in the cylinders heats up and passes a gaseous phase, leading to the need to use ventilation systems of the liquid H₂ storage tanks [10].

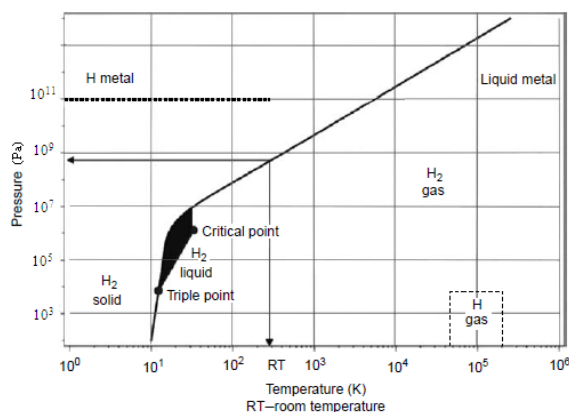


Fig. 1. Phase diagram of hydrogen, adapted from Ref. [9]

In the specialized literature, an experiment was presented in which a mixture of H₂ (in a gas furnace), and liquid nitrogen, showed a fairly high density, at temperatures higher than the temperature at which hydrogen is liquid. Valorially, it was shown that a mixture with 70 mol% H₂ has a density of 45 kg H₂/m³, at a temperature of 77 K and a pressure of 41.3*10⁶ Pa [11].

3.3. Storage in the form of metal hydrides

Metal hydrides are systems having the ability to store H₂, at high temperatures and release it in the form of gas in order to be used as fuel. This reaction is carried out by heating metal hydrides at various high temperatures. Metal hydrides present an advantage, from the point of view of stored hydrogen, compared to storing H₂ in the form of gas or liquid, having a storage capacity of 0.13-0.15 kg H₂/L. The simplest metallic and intermetallic alloys, such as

LaNi or FeTi, can react with hydrogen at low temperatures (100 °C) and low H₂ pressures. The mass percentage of H₂ in the case of these metal hydrides varies between 1.5% and 3%, and the hydrogen density per volume is between 0.05-0.12 kg H₂/L [6]. Greater hydrogen storage capacities are found in materials such as Mg and MgNi, which form hydrides at temperatures of approximately 300 °C and H₂ pressures between 5*10⁵-10⁶ Pa. Although metal hydrides present advantages from the point of view of the high amount of H₂ stored in the volume unit, their problem is the relatively long time required to carry out the hydride-dihydride processes [9].

In 1998, in Augusta, Georgia, a bus that used hydrogen as fuel was implemented for the transportation of people. The hydrogen storage system consisted of a lanthanum-nickel-aluminium metal alloy, which can be hydrogenated at low temperatures and provides 6 kg of H₂/h, ensuring the vehicle an autonomy of 300 km [12].

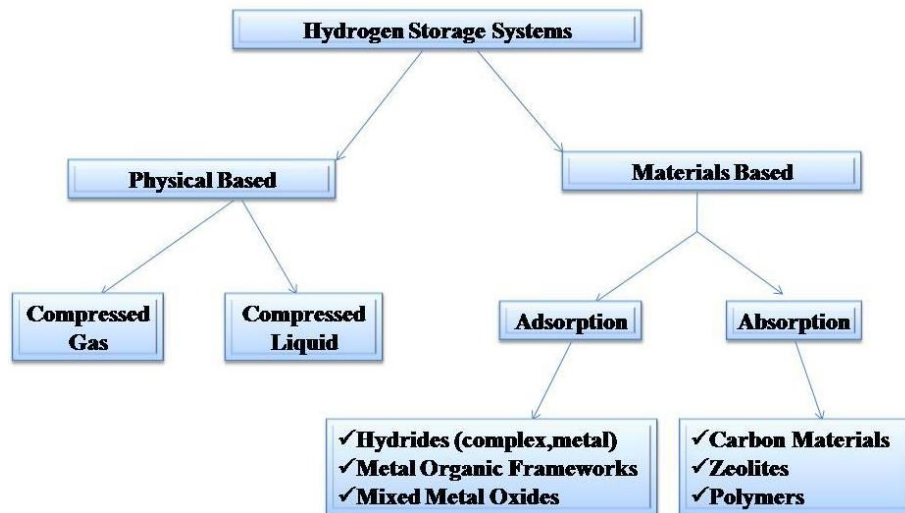


Fig. 2. Hydrogen storage systems, adapted from Ref. [10]

4. Storage of hydrogen in the form of hydrides

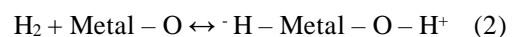
4.1. General information about hydrogen storage in materials

Chemical reactions of H₂ are of interest in fields such as chemistry or the use of hydrogen as a fuel. It is known that at a pressure of 10⁵ Pa, H₂ passes from a gaseous state to a liquid state. If an electrical discharge is applied to hydrogen gas at low pressure, reactions such as molecular dissociation, ionization or recombination occur. These effects favour the formation of molecular hydrides, saline hydrides or metallic hydrides [13].

Molecular hydrogen can be separated by homolytic or heterolytic processes in contact with metals, metal oxides or a mixture of activated metal oxides. The homolytic dissociation results from the absorption of hydrogen by the substrates of the activated metal, according to the equation:



while the heterolytic dissociation reaction in H⁺ and H⁻ is found in the case of metal oxides [10], according to the equation:



Storing hydrogen in metals is one way that hydrogen can be released later to be used as fuel for combustion engines or batteries. Hydrogen can be stored in underground reserves, in large quantities, or in cylinders for storage in small quantities. The electrochemical storage of hydrogen in the form of batteries has the highest yield among all methods of storing this gas [14].

According to the Office of US Energy Efficiency and Renewable Energy, the technical requirements of a hydrogen storage system for vehicles are in Table 2.

Table 2. Requirements for hydrogen storage systems in the form of hydrides [15]

Storage parameter	Unit	2020	2025
Usable, specific energy from H ₂	kWh/kg	1.5	1.8
Usable energy density from H ₂	Kwh/L	1.0	1.3
Storage system cost	\$/kWh net	10	9
Operating ambient temperature	K	233/253	233/253
Min/max delivery temperature	K	233/358	233/358
Operational cycle life	Cycles	1500	1500
Min delivery pressure from the storage system	Pa	5*10 ⁵	5*10 ⁵
Max delivery pressure from the storage system	Pa	12*10 ⁵	12*10 ⁵
Onboard efficiency	%	90	90
System fill time	min	3-5	3-5
Average flow rate	(g/s)/kW	0.004	0.004

Hydrogen fuel cells work just like batteries, they generate electricity based on an electrochemical reaction. A fuel cell needs three primary elements:

hydrogen, oxygen and electrolyte. H₂ and O₂ chemically react forming water. In a fuel cell, there is no combustion process. The electrons released as a result of the chemical reaction produce an electric current through an external circuit [14].

4.2. Types of hydrides

Hydride means a binary system, in which hydrogen forms compounds with other elements from the periodic table (E_a-H_b). Usually, hydrides fall into three major categories: ionic, covalent, and metallic.

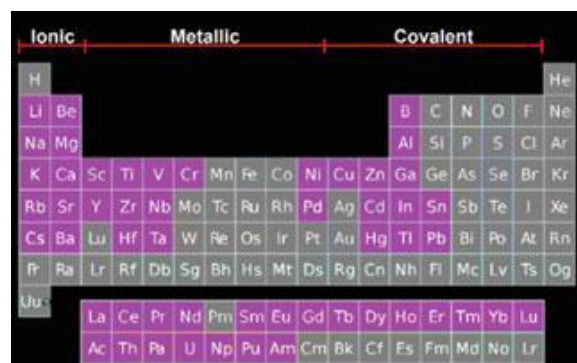
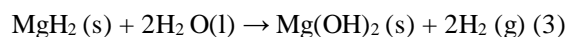


Fig. 3. The ability of materials to form hydrides, adapted from Ref. [14]

1. In the case of ionic hydrides, hydrogen compounds together with the most electropositive metals (especially alkali and alkaline metals) form ionic hydrides by releasing H₂ in contact with Brønsted acids and transferring H⁻ to electrophiles. This category of hydrides is also known as saline hydrides or pseudohalides. Ionic hydrides of the heaviest elements react violently with water and generate H₂ according to the reaction [14]:



2. Covalent (complex) hydrides, the hydrogen atom reacts with one or more nonmetals. Hydrogen forms covalent bonds with an electropositive element by giving up pairs of electrons. AlH₃, BH₃, BeH₂ are some examples of complex hydrides. However, BH₃ and AlH₃ are very unstable, because they form complex anion in combination with hydride anion. The most common situations are tetrahydridoborate (NaBH₄) and lithium tetrahydridoaluminate (LiAlH₄) [14].
3. Metal hydrides, also called interstitial hydrides, can be produced by the reaction of hydrogen with transition metals. Their specific

structure allows them to be non-stoichiometric, with variable composition. Using this idea as a basis, a crystalline network can be developed in which hydrogen atoms can fill the space in the structure and not in a well-defined order. The reaction of interstitial hydrides with H₂O can produce H₂, according to the following equation [14]:



5. Metal hydrides

Metal hydrides are found in solid form, are non-stoichiometric and have a good thermal conductivity. Metal hydrides, salts, intermediates and binary metal hydrides have been found, but there are also some elements, such as ruthenium, which do not form binary hydrides, but form complex metal hydrides. Since the 1970s, several alloys have been developed that have the ability to store hydrogen. These metal-hydrogen systems have the following general form: 1. AB₅; 2. AB₃; 3. A₂B₇; 4. AB₂; 5. AB; 6. A₂B; where A is the metallic element that absorbs hydrogen and B is an element with poor hydrogen absorption qualities, but with increased catalytic activity. The secondary element is very important in the hydrogen dissociation process.

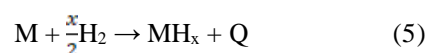
Metal-hydrogen bonds can be electrophilic or nucleophilic. The characteristics of the primary metal and the reaction conditions determine the properties of the metal hydrides obtained. Metal hydrides can be synthesized by metal protonation, oxidative addition of H₂, the addition of nucleophilic main-group hydrides (borohydrides, aluminium hydrides and silanes) and elimination of β-hydrides. Metallurgical techniques are most often used to obtain metal

hydrides, and chemical processes are generally used to produce complex hydrides. The process of metallurgical hydride formation includes the activation of hydrogen absorption (through hydridation/dehydridation treatments) [14].

A wide range of metal alloys can be used as hydrogen storage systems. Some metal hydrides have a volumetric density, which is about 115 kg/m³ (characteristic value of LaNi₅), but the disadvantage of such systems is the high reaction temperature. Although hydrogen is absorbed under certain conditions (temperature, H₂ pressure, etc.) by some metals and metal alloys, this gas can be released from the metal hydrides obtained, and the metal or alloy from which the hydrogen was extracted is also recovered. Metal hydrides show a favourable character regarding hydrogen storage. Metal-H systems with light elements (such as Li, Be, Na, B and Al) are reliable materials in the field of hydrogen storage, especially considering that the H: Metal ratio is greater than or equal to 2 [14].

5.1. Thermodynamic properties of metal hydrides

Most metal hydrides are formed by exposing metals/metal alloys to hydrogen gas at certain temperatures and pressures. As previously presented, the formation reaction of metal hydrides is:



where Q is the heat released during the hydrogenation reaction. The thermodynamic properties of the reaction are described by pressure-composition isotherms (PCIs) [16].

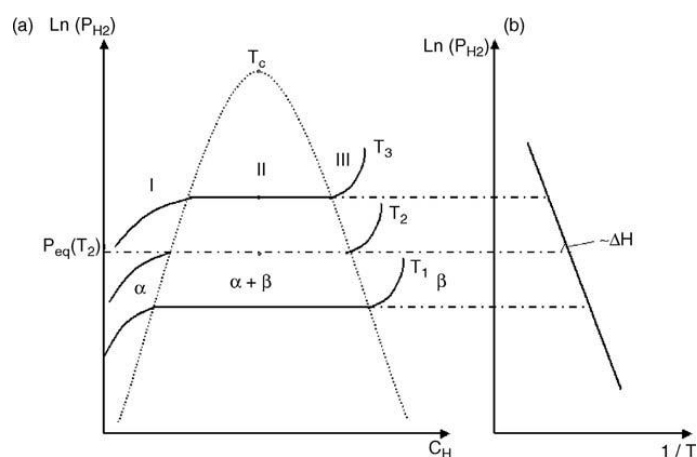


Fig. 4. (a) Schematic representation of the pressure-composition isotherm, where α is the solid solution of H₂ and β is the hydride phase [16]; (b) Van 't Hoff plot giving the enthalpy of hydride formation ΔH [16]

At low concentrations (below 1), hydrogen dissolves in the metal structure and forms a solid phase solution (α). After that, the hydrogen is randomly distributed in the metal and its concentration varies slightly depending on the temperature. The α phase has the same structure as the base metal. The thermodynamic equilibrium condition is given by the formula:

$$\frac{1}{2}\mu_{H_2}(p, T) = \mu_H(p, T, c_H) \quad (6)$$

where μ_{H_2} is the chemical potential of molecular hydrogen, μ_H is the chemical potential of atomic hydrogen in the metal and c_H is the hydrogen concentration (H/Metal ratio), being expressed as the number of hydrogen atoms per number of metal atoms [16].

As H_2 pressure increases, the concentration increases until the H-H interaction becomes important. At this moment, a phase with a high concentration (β phase) appears in H_2 . The system now has 3 types of phases (α , β and hydrogen in gas form) and two components (metal and hydrogen). From the Gibbs phase law, the degree of release is:

$$f = C - P + 2 \quad (7)$$

where C is the number of system components and P is the number of phases. It can be concluded that, in a two-phase region, the concentration increases while the hydrogen pressure is constant. When phase α disappears completely and phase β is found exclusively in the system, the system has two degrees of release. Hydrogen penetrates the solid material, in the β phase, and its pressure increases with the concentration [16].

5.1.1. Thermodynamics at low concentration

At low pressures ($P < 10^7$ Pa), hydrogen has the properties of an ideal gas and its chemical potential is given by the relation [16]:

$$\frac{1}{2}\mu_{H_2} = \frac{1}{2}H_{H_2}^0 - \frac{1}{2}TS_{H_2}^0 + RT\ln p_{H_2}^{1/2} \quad (8)$$

where $H_{H_2}^0$ and $S_{H_2}^0$ are the standard enthalpy and entropy. The chemical potential of the dissolved H atom is [16]:

$$\mu_S = H_S - TS_S^{id} + RT\ln\left(\frac{c}{b-c}\right) \quad (9)$$

where H_S is the enthalpy, and S_S^{id} is the non-configurational part of the entropy of hydrogen in the solid alloy. The last element in the equation is the configurational part of entropy, where b is the number

of interstitial spaces per metal atom and c is the number of spaces occupied by hydrogen atoms. The equilibrium condition equation can be expressed as follows [16]:

$$\Delta H_S - T\Delta S_S = RT\ln p^{1/2} + RT\ln\left(\frac{b-c}{c}\right) \quad (10)$$

where:

$$\Delta H_S = H_S - \frac{1}{2}H_{H_2}^0 \quad (11)$$

$$\Delta S_S = S_S^{id} - \frac{1}{2}S_{H_2}^0 \quad (12)$$

In the case of less dense solutions ($c < b$), the equilibrium condition is described by Seivert's Law, which is Henry's simple law for the dissociation of solutions [17]:

$$p_{H_2}^{1/2} = K_S \quad (13)$$

where K_S is a constant equal to:

$$K_S = \exp\left\{\frac{1}{RT}(\Delta H_S - T\Delta S_S - RT\ln b)\right\} \quad (14)$$

Seivert's law is valid because hydrogen in gaseous form has the properties of an ideal gas and its molecules are dissociated into atoms before being dissolved in metals [16].

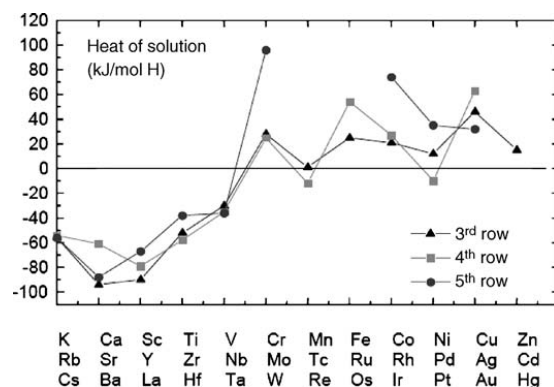


Fig. 5. The value of the heat of solution for the elements on rows 3, 4 and 5 of the periodic table, according to Ref. [16]

Figure 5 shows the values of the heat of dissolution for alkali, alkaline earth and transition metals. It is observed that the values for heat are the same for the first three rows of elements in the periodic table. This fact demonstrates how the heat of solutions is determined by the coarse electronic structure of the host metal [16]. From the point of view of the entropy, the biggest contribution is the

configurational entropy loss of gaseous hydrogen and it is approximately constant for all metals ($\Delta S_s \approx -65 \text{ kJ (molH)}^{-1}$) [16].

5.1.2. Thermodynamics at high concentration

Usually, the heat of the solution is a function of the hydrogen concentration. For high concentrations, the equilibrium pressure P_{eq} for phase transformation $\alpha \rightarrow \beta$ is given by Van't Hoff's law:

$$\ln P_{eq} = \frac{\Delta H}{RT} - \frac{\Delta S}{R} \quad (15)$$

where ΔH and ΔS are the enthalpy and entropy of the $\alpha \rightarrow \beta$ transition [16].

In most cases, the change in entropy is given by the loss of standard entropy of hydrogen gas upon contact with the metal structure. Considering this aspect, it can be concluded that the entropy term is not considerably dependent on the nature of the metal and that the ΔS term is considered constant. For enthalpy calculations, H-H interactions must be taken into account. We consider that the formation enthalpy (ΔH) of the β phase varies linearly with the hydrogen concentration. The dependence of the enthalpy on x can be written in the form [18]:

$$\frac{\partial \Delta H}{\partial x} = \left(\frac{\partial \Delta H}{\partial V} \right) \times \frac{\partial V}{\partial x} + \left(\frac{\partial \Delta H}{\partial x} \right) v \quad (16)$$

where:

$$\left(\frac{\partial \Delta H}{\partial V} \right) \times \frac{\partial V}{\partial x} \approx -\gamma K_0 \frac{v_H^2}{v_0} = -u_{els} \quad (17)$$

and v_0 is the atomic volume, v_H^2 it is the increasing volume per hydrogen atom (usually between 2 and 3 Å [19]), K_0 is the bulk modulus and γ is expressed by the relation [16]:

$$\gamma = \frac{2(1-2\sigma)}{3(1-\sigma)} \quad (18)$$

where σ is Poisson's ratio. In general, K_0 is approximately constant with hydrogen concentration. Therefore, for a certain metal, the elastic contribution can be considered constant [16].

6. Intermetallic hydrides

Most of the elements in the periodic table can form hydrides. As can be seen in Figure 6, their dissociation pressures and temperatures are not practical in most applications (temperature between 273-373 K and hydrogen pressure between 10^5 - 10^6

Pa). Vanadium is the only element that meets these conditions, but the hydrogen release capacity is still too low. All these aspects have led to the development of various alloys that meet these conditions and can be applied in practical activities. Compared to the metal-hydrogen system, the alloy-hydrogen system is more complex, because the interstitial spaces have a different chemical and geometric configuration [16].

The first system intended for the formation of intermetallic hydrides was the ZrNi alloy [20]. Later, other magnesium-based alloys were developed that showed an increased potential in hydrogen storage (such as the Mg_2Ni alloy) [21]. After that, the development and elaboration of hydrides that can be activated at room temperature, such as the ternary systems $TiFeH_2$ or $LaNi_5H_6$ began. After the appearance of these ternary systems, a large number of intermetallic hydrides were studied. Compared to metallic hydrides, intermetallic hydrides show increased hydride stability [16].

Generally, intermetallic compounds are formed by combining a metal that easily forms stable hydrides (A) with an element that forms unstable hydrides. Taking into account these aspects, intermetallic compounds can be grouped according to their stoichiometry [16]: 1. AB_5 ($LaNi_5$, $CaNi_5$); 2. AB_2 ($ZrMn_2$, ZrV_2); 3. AB ($TiFe$); 4. A_2B (Mg_2Ni).

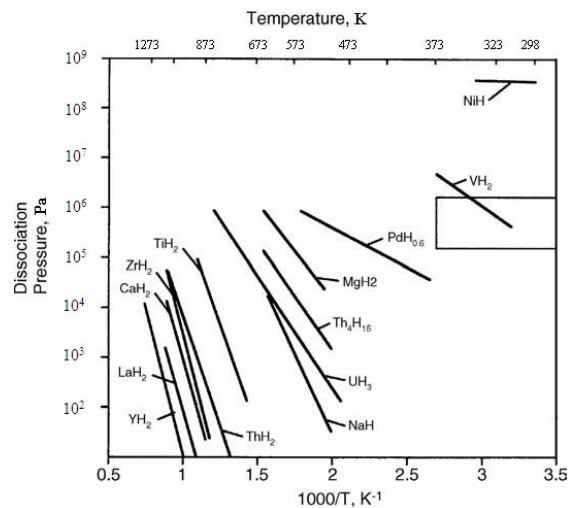


Fig. 6. Diagram for the dissociation pressure, as a function of temperature and pressure, for some fundamental hydrides, adapted from Ref. [16]

6.1. Crystal structure

Ternary hydrides have a different crystal structure with varying symmetries. In most cases, as the hydridation of two-element alloys takes place, the structure expands and deforms, but the crystal structure remains unchanged. However, for some

hydrides of TiFe, Mg₂Ni, CaNi₅ and LaNi₅ alloys, the crystal structure changes according to the hydrogen content. During the hydrogenation treatment, hydrogen atoms occupy specific interstitial spaces. From the point of view of geometric and calculation aspects for different hydrogen concentrations in hydrides using AB₂ type alloys, the rule was developed that the hole size is a minimum of 0.4 Å, while the minimum bond distance between hydrogen atoms is 2.1 Å. There are some systems that are an exception to this rule and have shown differences due to the difficult structure, determined using neutron diffraction [16].

6.2. Electronic structure

The hydride treatment changes the electronic structure of the alloys, these changes can be divided into four categories [22]:

1. the change of electron symmetry and the reduction of the bandwidth caused by the expansion of the crystal structure;
2. the appearance of a hydrogen-metal bond band below the d-band of the metal. Electrons are transferred from the sd band to the new band and some metal states can be pulled below the Fermi level;
3. in hydrides with more hydrogen atoms per measure unit, the HH interaction produces new attributes in the lower portion of the density of states;
4. the general rise above the Fermi level is caused by the inequality between the additional electrons brought by hydrogen and the number of new electron states.

6.3. Practical aspects for the use of intermetallic hydrides

In order for intermetallic hydrides to be used on a large scale, transportation, energy systems, etc., certain aspects must be taken into account [16]:

1. alloy/hydride fabrication, if an alloy is synthesized, the next important aspect is activation;
2. activation must be carried out under conditions as similar as possible to thermodynamic equilibrium;
3. hydride/dihydride treatments must be carried out at low pressures and temperatures (from this point of view, metal hydrides are more advantageous than conventional H₂ storage methods);
4. the amount of hydrogen that can be stored by the metal alloy;
5. alloy strength.

6.3.1. The development of alloys

As more and more complex hydrides are developed (nanocrystalline, multi-element systems, composites and nanocomposites, graphite/metals or similar hybrid systems, clusters, etc.), it is necessary to take into account the fact that for practical applications, a considerable amount of such materials is needed. However, laboratory technology allows testing and development in this field, which allows obtaining new compounds. When a favourable material for hydrogen storage is found, it will face industrial-scale fabrication [16].

6.3.2. Activation of the materials

In order to achieve the activation of metals, we must not neglect the fact that metals can present an oxide layer on the surface, of different thicknesses, which varies depending on the oxidation process of each metal element. This oxide layer acts as a barrier that blocks the interaction of hydrogen with the metal, so it must be removed before hydridation to allow hydrogen gas to come into contact with the material. Considering these aspects, metal activation is recommended to be performed at elevated hydrogen temperatures and pressures, to force hydrogen particles to penetrate the oxide layer and contact the metal. Simultaneously with hydridation, the volume of the material structure increases, and during the dehydration treatment, it returns to its original dimensions. This expansion-contraction process breaks the metal particles, exposes a new metal surface and reduces the particle size [16].

As an example, for the metal alloy Mg₂Ni, it has been demonstrated in the literature that the activation process is more reliable if mechanical grinding processes were previously performed on the surface of the material [23].

In practical applications, if the material intended for hydrogenation is embedded in a hydrogen storage device, it must be taken into account that the materials from which the respective system is made have considerable resistance at high temperatures and high pressures [16].

6.3.3. Hydrogen release capacity

In the case of practical applications, the dehydration process is very important. It is characterized by the reversibility capacity $\Delta(H/Metal)$ being defined as the bearing width. The reversibility capacity can be considered lower than the maximum capacity $(H/Metal)_{max}$ [24]. A classic example is vanadium hydride. At 353 K, vanadium forms monohydride VH_x ($x \approx 1$) at hydrogen pressure

between 10^{-6} – 10^{-7} MPa. At higher pressures (around 1 MPa), vanadium dihydride (VH_x , $x \approx 2$) is obtained [16]. In practical applications, the dehydrogenation of vanadium monohydride cannot be realized and it can be concluded that hydrides of the type VH_x ($1 < x < 2$) show reversibility. The hydrogen storage capacity can be expressed either in the form of atomic ratio (H/Metal) or by mass percentages (wt.%) [16]. The atomic ratio is the number of hydrogen atoms stored per metal atom. The mass percentage represents the amount of hydrogen stored in the hydrate material [16].

6.3.4. Hydrogenation kinetics

Hydrogenation is a complex process in which the gas molecules are divided into atoms that form bonds with the crystalline structure of the metal hydride. The overall kinetics is limited by the slowest step, called the rate-limiting step. For the research and development of new alloys, it is recommended that the transported mass and heat do not constitute the speed-limiting step [25]. Taking into account these aspects, it should be considered that the design of the sample ensures a maximum value of thermal conductivity and a minimum value for the resistance to the flow of hydrogen [16].

For the characterization of metal hydrides, the kinetic curve for a given reaction is the transformed fraction as a function of time. The dependence of the curve on pressure and temperature must be studied to deduce the rate-limiting steps of the reaction. For the hydrogen-metal system, the situation is more complicated due to the heat of the reaction, the fast reaction rate, and the low thermal conductivity of the hydride phase. Other factors that can influence the hydridation kinetics curve are sample size, particle size, surface properties and metal and gas purity [16].

7. Conclusions

Hydrogen is a clean energy source of high interest in contemporary times. Currently, several H_2 production projects are being debated, with the aim of being used as an energy source in industries such as transport, heat generation and electricity production. Starting from 2022, H_2 -powered vehicles are used and sold in Australia. They have an autonomy of 900 km and a refuelling time of only 5 minutes.

At the global level, research and development works are continuously carried out for hydrogen storage and transportation systems, reliable from several points of view (safety, economics, etc.). Metal hydrides are more advantageous than conventional hydrogen storage in pressure vessels, because of the higher gas storage capacity per unit volume.

Also, in the process of developing an alloy intended for hydrogen storage, aspects such as the hydrogen storage capacity, the conditions under which the hydride reaction is carried out (temperature, H_2 pressure), the ability of the formed hydride to release hydrogen must be taken into account during dehydrogenation, life resistance to hydrogenation-dehydrogenation cycles, the possibility of being produced in industrial quantities, an easy production process, etc.

Taking into account the fact that hydrogen is considered to be a favourable energy source for the future, further global research, development, testing and implementation of hydrogen storage and transportation systems are needed.

References

- [1] **Bahman Zohuri**, *Hydrogen Energy. Challenges and Solutions for a Cleaner Future*, 2019.
- [2] **Schlapbach L., Anderson I., Burger J. P.**, *Hydrogen in Metals, Electronic and Magnetic Properties of Metals and Ceramics*, Part II, 3B, 1994.
- [3] **Chen C. P., Siu B. H., Li Z. P. et al.**, *Z. Phys. Chem. NF*, 181, 259, 1993.
- [4] **Gerard N., Ono S.**, *Hydride formation and decomposition kinetics*, in *Hydrogen in Intermetallic Compounds II*, 67, 1999.
- [5] **Sandrock G.**, *J. Alloy Compd.*, p. 293-295, 877, 1999.
- [6] **Zanfir M., Gavrilidis A.**, *Catalytic combustion assisted methane steam reforming in a catalytic plate reactor*, *Chemical Engineering Science*, 58, 2003.
- [7] **Haussinger Peter, Lohmuller Reiner, Watson Allan M.**, *Hydrogen, 1. Properties and Occurrence*, Ullmann's Encyclopedia of Industrial Chemistry, 2011.
- [8] **Kaveh Mazloomi, Nasri B. Sulaiman, Hossein Moayedi**, *Electrical Efficiency of Electrolytic Hydrogen Production*, *International Journal of Electrochemical Science*, 7, 2012.
- [9] *******, <https://www.hydrogenfuelnews.com/nanogalvanic-aluminum-powder-generates-hydrogen-without-a-catalyst/8536799/>.
- [10] *******, www.irena.org.
- [11] *******, www.energy.ec.europa.eu/topics/energy-systems-integration/hydrogen_en.
- [12] *******, www.energyindustryreview.com/enviroment/h2-production-projects-in-romania-ahead-of-governments-strategy/.
- [13] **Ram B. Gupta**, *Hydrogen Fuel. Production, Transport, and Storage*, 2009.
- [14] **Burke A. F., Gardner M.**, *Hydrogen Storage Options: Technologies and Comparisons for Light-Duty Vehicle Applications*, Research Report UCD-ITS-RR-05-01, Institute of Transportation Studies, University of California, Davis 2005.
- [15] **Berry G. D.**, *Hydrogen Absorption in Fluids: An Unexpected Solution for Onboard Hydrogen Storage*, UCRL-TR-209650.
- [16] **Jacobs W., Heung L., Motyka T., Summers W. et al.**, *Final Report for the H_2 Fuel Bus*, SAE Technical Paper, 1999-01-2906, 1999.
- [17] **Rana Mohtadi, Shinichi Orimo**, *Nature Reviews Materials*, 2, 2017.
- [18] **Ali Salehabadi, Mardiana Idayu Ahmad, Norli Ismail, Norhashimah Morad, Morteza Enhessari**, *Energy, Society and the Environment*, Solid-State Hydrogen Storage Materials, 2020.
- [19] *******, www.energy.gov/ure/fuelcells/doe-technical-targets-onboard-hydrogen-storage-light-duty-vehicles.
- [20] **Michael Hirscher**, *Handbook of Hydrogen Storage: New Materials for Future Energy Storage*, 2010.



[21]. Wiswall R., *Hydrogen Storage in metals*, Hydrogen in Metals II, 29, 1978.
[22]. Fukai Y., *The Metal-Hydrogen System*, Materials Science, 2nd ed., vol. 21, 2005.

[23]. Fukai Y., J. Less Common, Phys. Chem., 76, 8, 1991.
[24]. Ashby E. C., Brendel G. J., Redman H. E., Inorganic Chem., 2, 499, 1963.
[25]. Sklar N., Post B., Inorg. Chem., 6, 699, 1967.

REGARDING THE USE OF FINITE ELEMENT MODELING FOR PROPULSION SYSTEM SIZING IN V.T.O.L. DRONES

Adrian LEOPA

"Dunarea de Jos" University of Galati, Engineering and Agronomy Faculty of Braila, Romania
e-mail: adrian.leopa@ugal.ro

ABSTRACT

At the moment, VTOL drones have proven their efficiency in several areas, for this reason, they have become indispensable tools for a large category of applications. This paper presents aspects related to the dimensioning stage of the propulsion system of a drone based on finite element modeling, to establish the traction force necessary to ensure sustentation.

KEYWORDS: drone, modeling, finite element

1. Introduction

Currently, VTOL drones (vertical take-off and landing) are used in various fields due to the multiple advantages they present: small size, vertical take-off/landing, flight in narrow spaces, high precision and others.

These are versatile systems that have found multiple uses, such as:

- monitoring environmental factors with high-precision sensors;
- assessment of soil quality and vegetation status of crops using multispectral cameras;
- crop herbicide;
- performance of cartographic and topographical tasks;
- objective surveillance missions;
- extinguishing fires.

As regards the monitoring of environmental factors, this is a vital activity from the perspective of ensuring a high level of human, animal and plant quality of life. For this reason, in some countries in urban agglomerations or areas bordering industrial zones, there are fixed weather stations for which they fulfil this role. However, for unforeseen situations such as natural or man-made disasters, there are several devices capable of measuring the concentrations of pollutants and transmitting this information to a decision-making forum.

In the agricultural field, VTOL drones have imposed themselves by drawing up orthophoto plans capable of providing useful information on soil quality parameters and crops of interest. Subsequently, the same type of drones can be used to treat crops differently based on previously made

orthophoto plans, thus achieving a saving of treatment substances.

In terms of surveillance of targets, VTOL drones can replace the human factor and can cover large areas both day and night.

In certain situations, these drones can be used to extinguish or isolate fires.

2. Aspects regarding the dimensioning of the propulsion system

Currently, there is a multitude of propulsion system configurations for VTOL drones, for this reason, the theoretical study presented in this paper has as its main objective the determination of flight parameters for a single bipal propeller.

In order to choose the propulsion system, the following steps were taken:

1. Establishing the program for numerical modelling;
2. Establishing the propeller model;
3. Modelling.

Due to its proven performance in the field of scientific research, the Ansys Workbench program was chosen as the medium for numerical modelling.

When choosing the propeller model, the following parameters should be considered: diameter, pitch, number of blades and its mass. The advantage of finite element modelling is that the above-mentioned parameters can be easily modified in order to characterize the dependence between them and flight parameters.

To describe the steps that were taken in order to evaluate the traction force developed by a twin blade

propeller of 15-inch diameter and 8-inch pitch, model taken from source [1].

3. Flow modelling in Ansys Workbench

From the Ansys program window, the Fluid Flow (Fluent) analysis system for airflow modelling

was chosen. Subsequently, from the menu of the Fluent system, the geometry environment opens in which the 3D model of the propeller is imported in the form of a file compatible with it.

In the next step, a "Rotor fluid" is created that will completely encompass the propeller, Fig. 2.

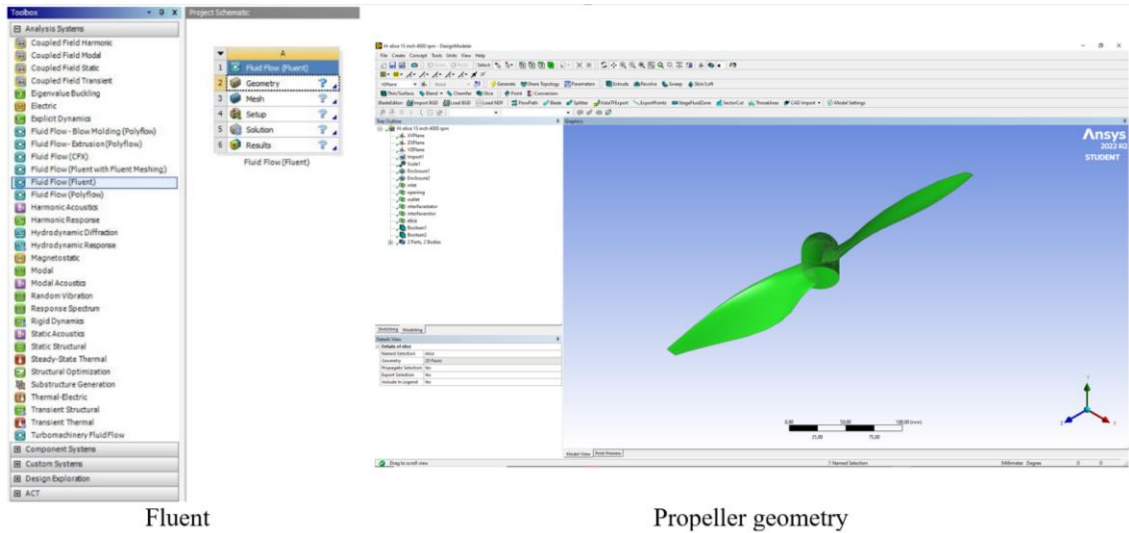


Fig. 1. Propeller geometry

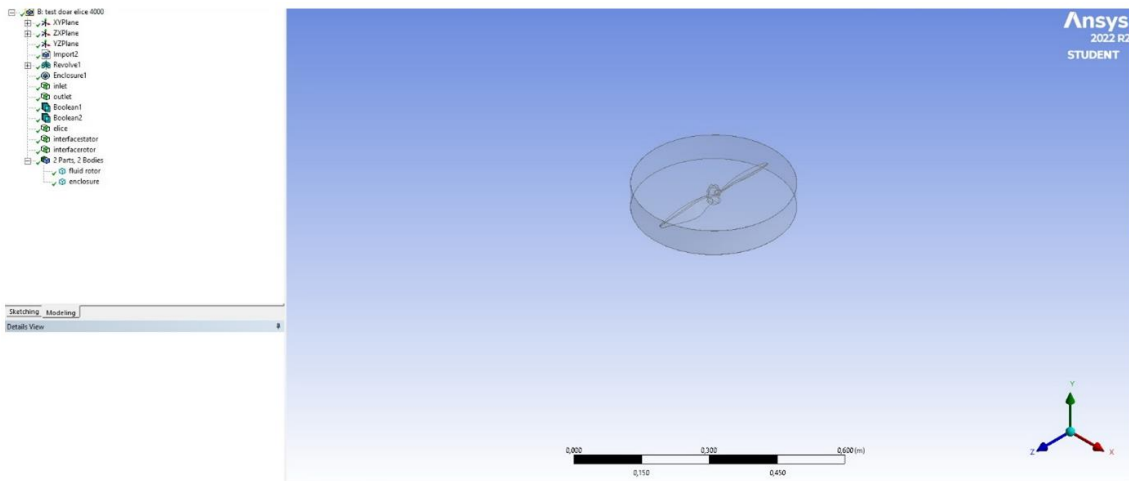


Fig. 2. Fluid rotor

The medium in which flow modelling will be done is created by defining a volume with the "enclosure" function and will be referred to as a "Fluid body".

Subsequently, the *rotor fluid* will be subtracted from the *fluid body* by calling the *boolean* function (*subtract*), but keeping the tool bodies. Then, the propeller will be subtracted from the rotor fluid with the help of the same Boolean function, this time without preserving tool bodies.

Once these steps are performed, we proceed to another stage in the same analysis system, namely: finite element model verification, and mesh module. At this stage, the previous model obtained will be discretized, Fig. 4.

After the verification stage with finite elements, the phase of establishing the analysis parameters is completed, in which the propeller material, speed, direction of rotation, environment in which it works and others are chosen.

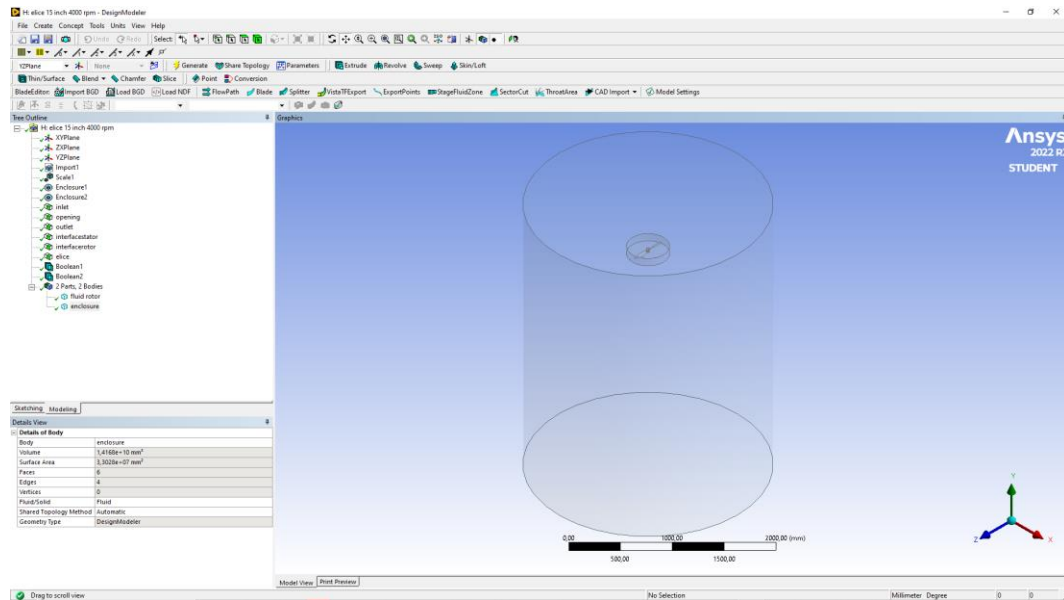


Fig. 3. Enclosure

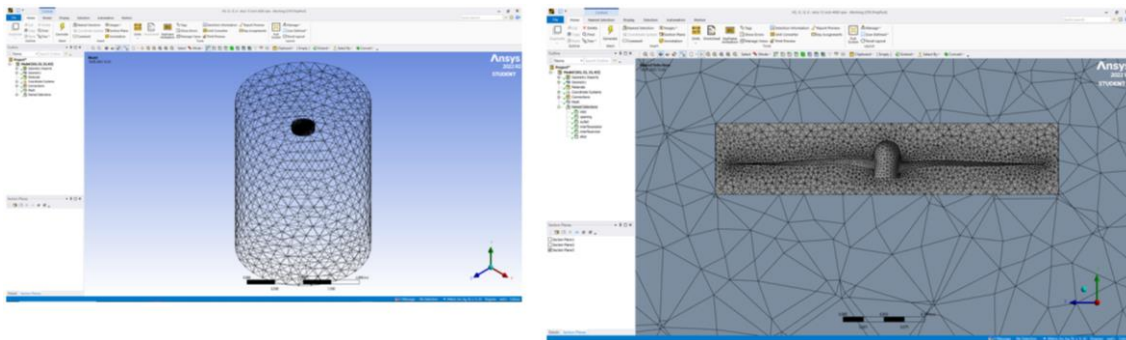


Fig. 4. Division into finite elements

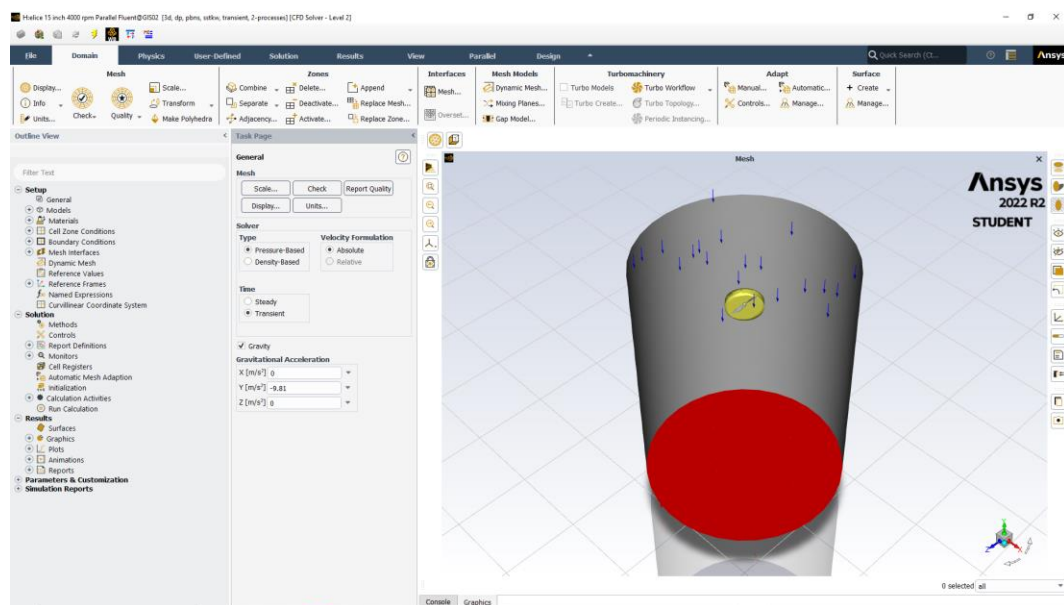


Fig. 5. Establishment of calculation factors

After solving the finite element model, variations in the obtained parameters are plotted as follows:

1. Figure 6 evaluates the speed variation during propeller operation at 7000 rpm, specifying the maximum value of 138.6 m/s;

2. Figure 7 shows the possibility of calculating the tractive force developed by the propellers, for the conditions considered this force being 35.4 N.

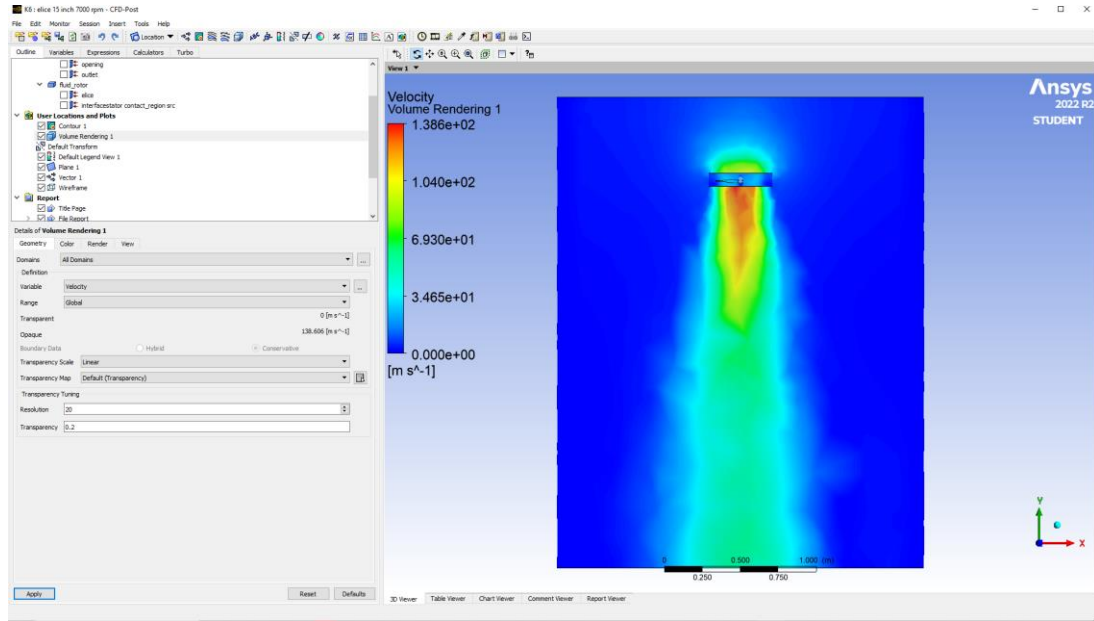


Fig. 6. Air flow

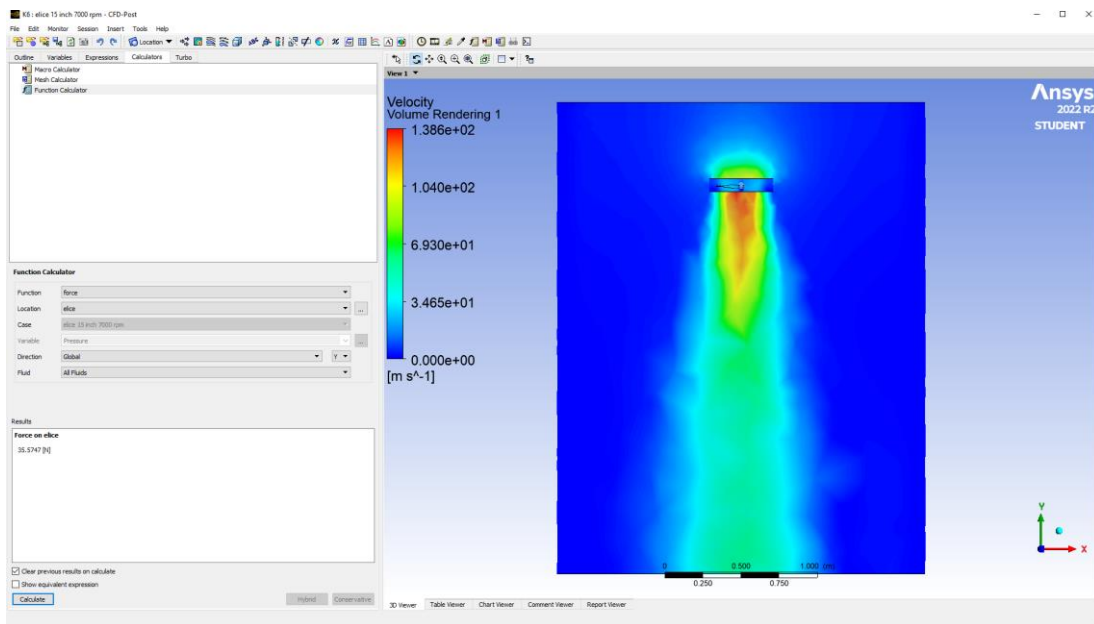


Fig. 7. Determination of traction force

The test of this propeller was carried out considering the following speed values: 4000, 5000, 6000 and 7000 rpm, given the dependence between

the thrust generated by the propeller and its speed is shown in Figure 8.

Based on dependency generated based on numerical modelling, Fig. 8, interpolation determines the function that best approximates the graph.

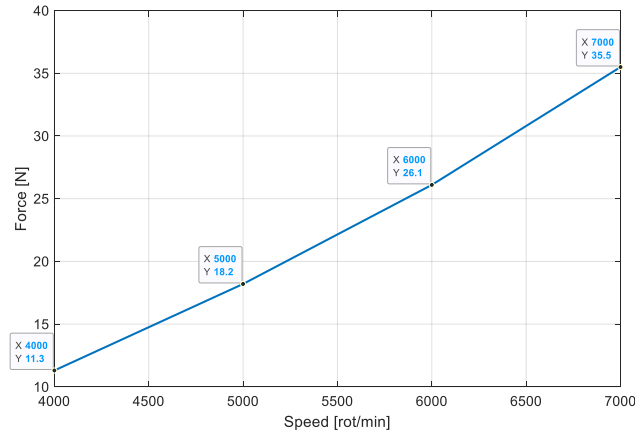


Fig. 8. Dependence between propeller speed and thrust generated

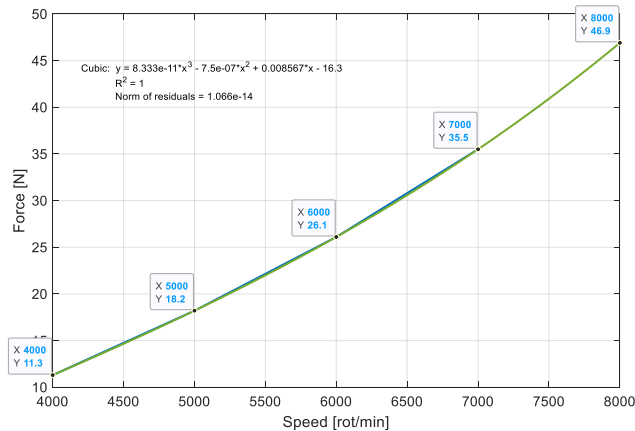


Fig. 9. Extrapolation of the dependence between propeller speed and generated thrust

The next step is to experimentally validate this dependence between thrust and propeller speed.

for high speeds is more expensive because the risks taken are higher.

4. Conclusions

This paper presents the steps to be taken to numerically model the operation of a propeller and, implicitly, determine the value of the traction force depending on its speed. If this dependence is subsequently experimentally validated, the tractive force can be estimated for higher speed values without having to run the experimental part. Although numerical modelling can be performed for any speed value, it should be noted that experimental validation

Acknowledgements

Thank you to Assoc. Prof. PhD Eng. Florin Nedelcuț for his guidance in understanding fluid flow modelling.

References

- [1]. ***, <https://grabcad.com/library/low-reynolds-propeller-for-ultra-light-aircrafts-1>.
- [2]. Silviu Butnariu, Gheorghe Mogan, *Analiza cu elemente finite în ingineria mecanică, Aplicații practice în ANSYS*, Editura Universității Transilvania din Brașov 20.

DETERMINATION OF STRESS CONCENTRATION FACTOR FOR A RECTANGULAR BAR WITH FILLET UNDER AXIAL LOADING: AN ARTIFICIAL NEURAL NETWORKS APPROACH

Doina BOAZU

Department of Mechanical Engineering, “Dunarea de Jos” University of Galati, Romania
 e-mail: doina.boazu@ugal.ro

ABSTRACT

Using computer techniques, stress concentration factors from the graphs can be converted into numerical values. Stress concentration factor values were collected in a database and an Artificial Neural Network (ANN) model can be developed for improving and extending the database. ANN model provides accuracy in obtaining the stress concentration factor values.

KEYWORDS: Stress Concentration Factor (SCF), Artificial Neural Network (ANN), axial loading

1. Introduction

The main objective is to develop an ANN model to properly predict the static stress concentration factor for a rectangular bar with fillet under axial loading.

In practice, the data for determining the stress concentration factor can be found in graphs that are obtained experimentally.

The determination of the stress concentration factor can be obtained using finite element simulation with optimization modules. The numerical finite element simulation is often time-consuming even quite accurate if the aim is to evaluate the stress-strain behaviour at the notched area [11].

The development of a simplified numerical model would prove effective to reduce the time needed to reach a good approximation of the stress concentration factor (K_t) for a proposed design (Ihsan TOKTAS1 and others, 2020).

Toktas *et al.* [11], developed an ANN model that provided high accuracy for the prediction of stress concentration factor (K_t) for a Crankshaft under Bending Loading.

2. Experimental background

The data for determining the stress concentration factor can be found in graphs that represent a formulation of the results of the experimental studies.

These graphs are still used these days to define the stress concentration factors. It is necessary to read

carefully the data in these curves when defining the stress concentration factor for a particular problem. These curves can be converted into numerical values. An ANN database was created using these data. A new ANN model was developed using Matlab software [14].

The precision measurements for axially loaded variable cross-section bars showed that in the case of cross-section variations, the stresses are not uniformly distributed on the surface of the cross-section [7].

The elements that influence the stress concentration factor (K_t) for a bar with a rectangular cross-section and a fillet is represented in Fig. 1. The bar has an applied axial force (tensile or compressive).

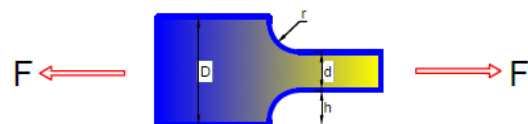


Fig. 1. Parameters involved in the calculation of the stress concentration factor. D = width of the larger section; d = width of smaller section; r = radius of fillet; t = bar thickness; F = applied force (tensile or compressive) [13]

The maximum stress σ_{max} is calculated as [13]:

$$\sigma_{max} = K_t \cdot \sigma_{nom} \quad (1)$$

Where K_t is the stress concentration factor that is determined from the Fig. 2, and σ_{nom} is calculated as [13]:

$$\sigma_{nom} = \frac{F}{d \cdot t} \quad (2)$$

The value of the stress concentration factor for rectangular bar fillet under axial loading is given by the formula [13]:

	$0.1 \leq h/r \leq 2$	$2 \leq h/r \leq 20$
C_1	$1.007 + 1.000\sqrt{h/r} - 0.031(h/r)$	$1.042 + 0.982\sqrt{h/r} - 0.036(h/r)$
C_2	$-0.114 - 0.585\sqrt{h/r} + 0.314(h/r)$	$-0.074 - 0.156\sqrt{h/r} - 0.010(h/r)$
C_3	$0.241 - 0.992\sqrt{h/r} - 0.271(h/r)$	$-3.418 + 1.220\sqrt{h/r} - 0.005(h/r)$
C_4	$-0.134 + 0.577\sqrt{h/r} - 0.012(h/r)$	$3.450 - 2.046\sqrt{h/r} + 0.051(h/r)$

$$K_t = C_1 + C_2 \left(\frac{2h}{D}\right) + C_3 \left(\frac{2h}{D}\right)^2 + C_4 \left(\frac{2h}{D}\right)^3 \quad (3)$$

Where the equation coefficients are calculated from Roark's formula for Stress and Strain, 8th Edition [12]:

The size of the coefficient K_t depends on the configuration and dimensions of the stress concentrators as well as the material of the piece. The stress concentration factors are the more dangerous

for the more fragile materials; if the material is tenacious, then the concentration effect is less important.

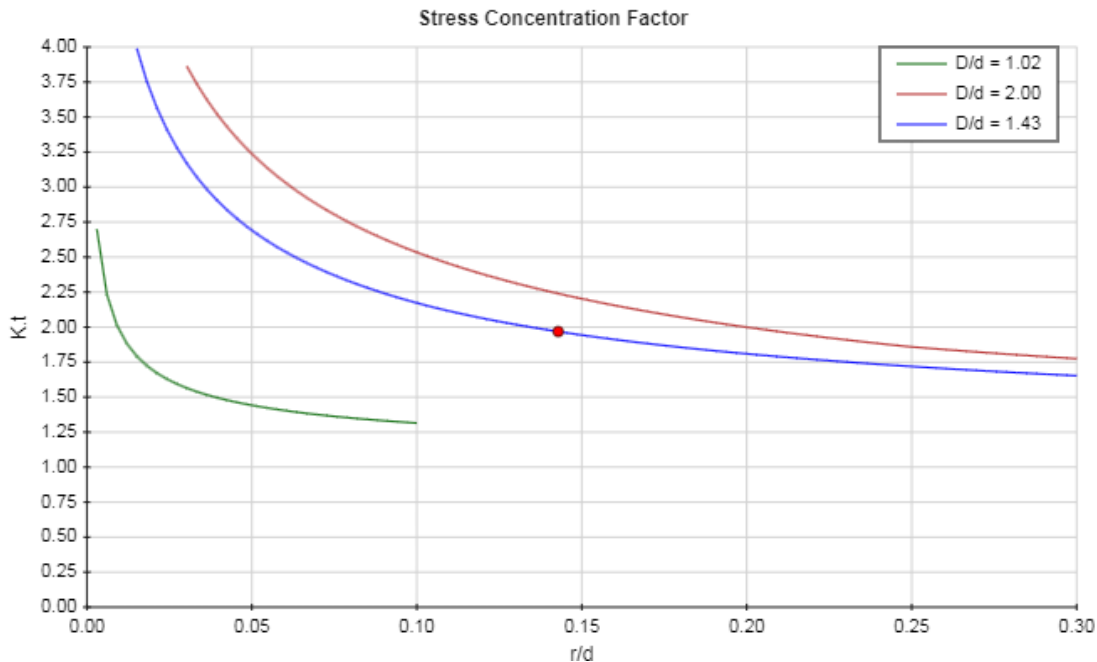


Fig. 2. Stress concentration factor [13]

The most important design variables are the ratio r/d , and ratio D/d as expressed in (Figure 1). These parameters are affected by the stress concentration factor.

The data used for training and testing ANN are given in Annex A and correspond to the following ranges of input variation:

- the $\frac{r}{d}$ varies in the range 0.01-0.09;

- for $\frac{D}{d}$ the following values were considered 1, 1.5 and 2.

3. Neural network modeling

An artificial neural network is a type of machine-learning process that uses interconnected

nodes or neurons in a layered structure that resembles the human brain (Fig. 3) [4].

This hierarchical network structure has an input layer receiving data from the outside and an output layer which sends final information to users. In the middle, hidden layers have no direct contact with the environment (Fig. 3).

As it has proved its efficiency for approaching non-linear functions [6], the Levenberg-Marquardt LM algorithm has been used for neural network training. Using notations in Figure 3, the output response is calculated using (eq. 4) [3]:

$$s = f(\sum w_i \cdot e_i + b) \quad (4)$$

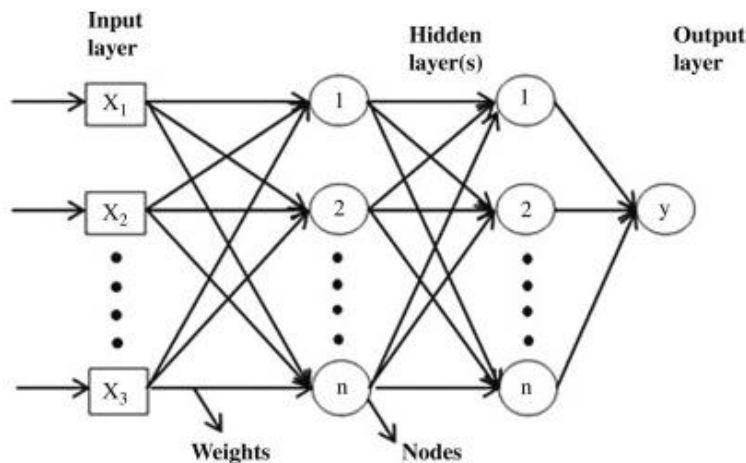


Fig. 3. An artificial neural network [4]

Two activation functions need first to be chosen: one applied in hidden layers and the second used in the output layer to determine the appropriate number of hidden neurons and output values. In practice it is used:

- Sigmoid function ($f(x) = 1/(1+e^{-x})$) in the hidden layer and;
- Linear function ($f(x) = x$) in the output layer (S.L.).

The Levenberg-Marquardt (LM) learning algorithm version was used at the training and testing stages of the Networks [14].

It is recommended that the number of hidden layers be 1-5, but many times good results can be obtained with a single hidden layer and in this sense, tests are made [11].

The hidden layers perform nonlinear transformations of the inputs entered into the network.

During training, weights “w” and biases “b” are initialized to small random values to avoid sharp saturation in activation functions “f”.

The main objective of this study is the development of an ANN numerical model to accurately predict the major element influence on the stress concentration factor for the rectangular bar with fillet axially loaded. Some major parameters used in the final ANN model have been optimized:

- the type of activation functions in hidden and output layers;
- the number of hidden layers;
- the number of neurons in the hidden layer.

One or two hidden layers are sufficient to solve any nonlinear complex problem.

In [1] two hidden layers are used to obtain the optimal Regression coefficient R for a nonlinear problem.

When any function contains a continuous mapping from one finite space to another, one has to make use of a single hidden layer [9].

The number of hidden layer neurons is 2/3 (or 70% to 90%) of the size of the input layer. If this is insufficient, then the number of hidden layer neurons can be added later on [1].

In specialized literature, calculation formulas for the number of neurons in a hidden layer are proposed; many of them use the number of tests as a variable in these formulas [9].

It is chosen a 2-4-1 ANN structure and the output response is calculated using the formula:

$$\text{output_response} = f\left(\sum w * \text{input_layer} + b\right) \quad (5)$$

Where “w” are the weights and “b” are biases and “f” are activation functions.

All numerical experiments were carried out using the MATLAB R2014b neural network toolbox [14].

Table 1. Tests in developing ANN structures and corresponding R-training values and Performance (Mean squared error)

ANN structure	R- training	Performance Mean squared error
2-2-1	0.98825 (Fig. 4a)	0.029472/118 epoch (Fig. 4b)
2-3-1	0.99704 (Fig. 5a)	0.007415/1000 epoch (Fig. 5b)
2-4-1	0.99945 (Fig. 6a)	0.0013558/ 1000 epoch (Fig. 6b)

The data for training and testing were determined using Roark’s formula [11].

The input and output variables are dimensionless quantities and therefore there is no need for their standardization to obtain a fast optimal Regression coefficient R.

The regression coefficients for training different ANN structures and performance from Table 1 are highlighted in Fig. 4-Fig. 6.

The data from Table 1 points out that the ANN selected model has a single hidden layer with 4 neurons.

Three coefficients are calculated to evaluate statistical network performance: RMSE, MAPE and linear regression coefficient R (Table 2).

The root means square error (RMSE) $RMSE = \sqrt{\frac{\sum_{i=1}^n \|y_i - \hat{y}_i\|^2}{n}}$

The mean absolute percentage error (MAPE)

$$MAPE = \frac{1}{n} \sum_{i=1}^n \left| \frac{\hat{y}_i - y_i}{y_i} \right| \times 100 \%$$

For linear regression coefficient R we used formula:

$$R = \frac{\sum_{i=1}^n (y_i - \bar{y})(\hat{y}_i - \bar{\hat{y}})}{\sqrt{\sum_{i=1}^n (y_i - \bar{y})^2 \cdot (\hat{y}_i - \bar{\hat{y}})^2}}$$

Where n is the number of observations, y_i is the actual value, \hat{y}_i is the predicted value, \bar{y} and $\bar{\hat{y}}$ are mean target and predicted output values. The values of coefficients calculated to evaluate the statistical network performance of the ANN model (Table 2) show its accuracy.

Table 2. Statistical Performance of Training ANN model

Linear regression coefficient	Root Mean Square Error (RMSE)	Mean absolute percentage error (MAPE) %
0.99945	0.0368	1.04

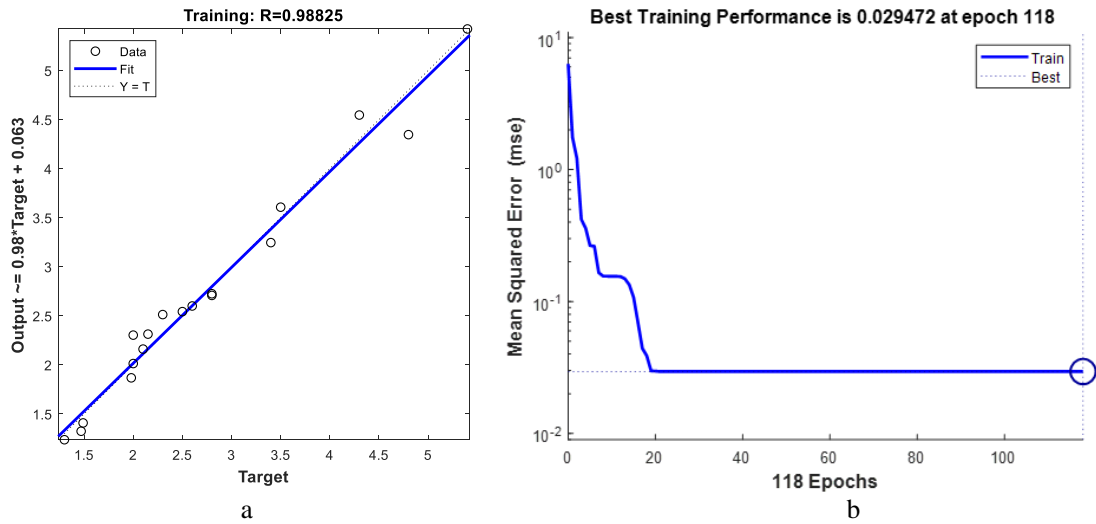


Fig. 4. a - ANN 2-2-1 Regression; b - ANN 2-2-1 Performance

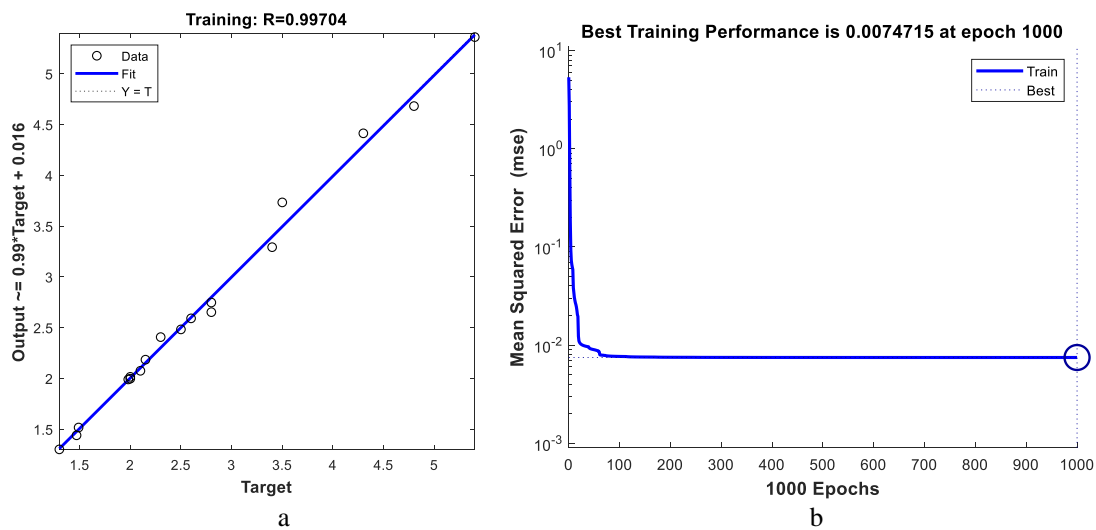


Fig. 5. a - ANN 2-3-1 Regression; b - ANN 2-3-1 Performance

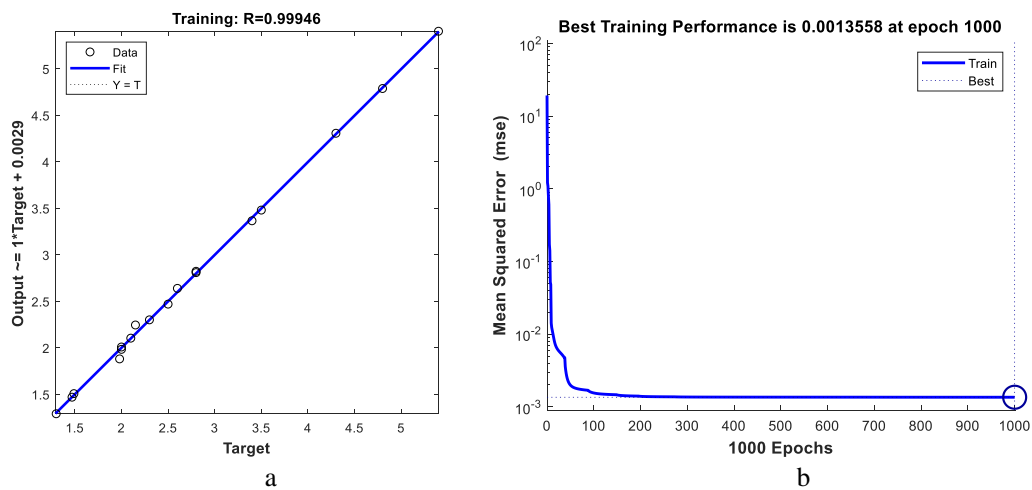


Fig. 6. a - ANN 2-4-1 Regression; b ANN 2-4-1 Performance

4. Prediction of static stress concentration factor

The Levenberg-Marquardt (LM) optimization algorithm has been used all along in this study to find out weights and biases.

The proposed ANN model has a single hidden layer with 4 neurons (Fig. 7).

Stress concentration factors K_t from experimental and predicted for training and testing data are given in Table 3 respectively in Table 4.

The graphic representation of the comparison between the experimental results and the predicted ones highlights the accuracy of the ANN model (Fig. 8 and Fig. 9).

The weights and biases values for the ANN model proposed are given in Table 5; with these values for weights and biases and taking into account the formula (5), values of the stress concentration factor K_t can be obtained for input data in the field in which the training was carried out.

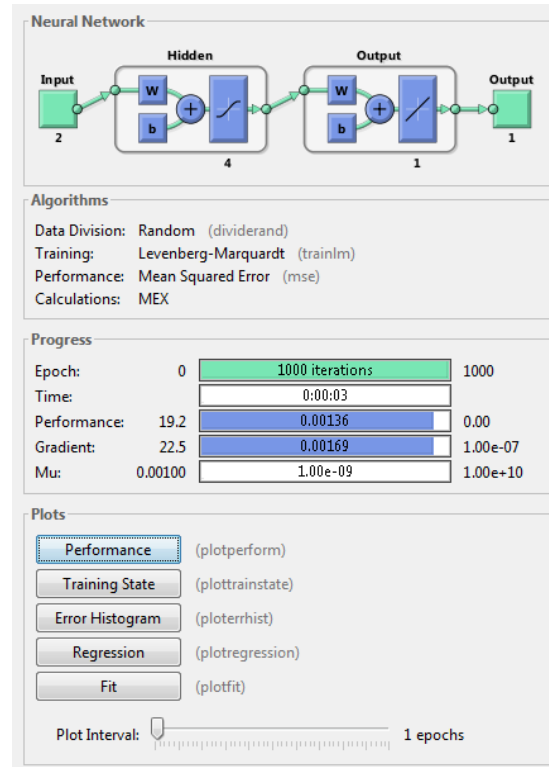


Fig. 7. ANN model using MATLAB

Table 3. Stress concentration factor K_t experimental and predicted for training data

Training data				
	$\frac{r}{d}$	$\frac{D}{d}$	K_t experimental	K_t predicted
1	0.01	1	2	2.0095
2	0.04	1	1.49	1.5082
3	0.05	1	1.47	1.47
4	0.09	1	1.3	1.2919
5	0.01	1.5	4.8	4.7887
6	0.02	1.5	3.5	3.4815
7	0.04	1.5	2.8	2.8234
8	0.06	1.5	2.15	2.2461
9	0.07	1.5	2.1	2.1047
10	0.08	1.5	2	1.9843
11	0.09	1.5	1.98	1.8817
12	0.01	2	5.4	5.4044
13	0.02	2	4.3	4.3075
14	0.04	2	3.4	3.3667
15	0.06	2	2.8	2.8093
16	0.07	2	2.6	2.6399
17	0.08	2	2.5	2.4706
18	0.09	2	2.3	2.3015

Table 4. Stress concentration factor K_t experimental and predicted for testing data

	Testing data			
	$\frac{r}{d}$	$\frac{D}{d}$	K_t experimental	K_t predicted
1	0.025	1	1.625	1.5154
2	0.075	1	1.375	1.2919
3	0.03	1.5	3	3.06
4	0.05	1.5	2.4	2.5381
5	0.07	1.5	2.1	2.1047
5	0.03	2	3.8	3.5779
7	0.05	2	3	3.0427

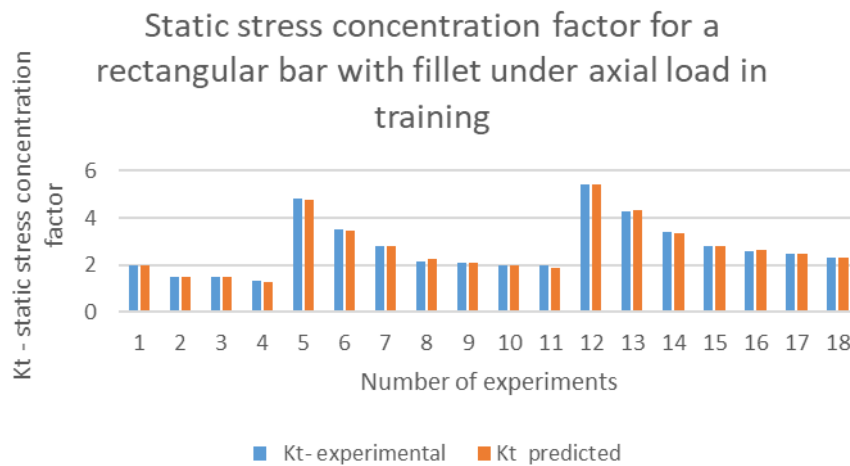


Fig 8. Stress concentration factor K_t for a rectangular bar with fillet Under Axial Loading, in training

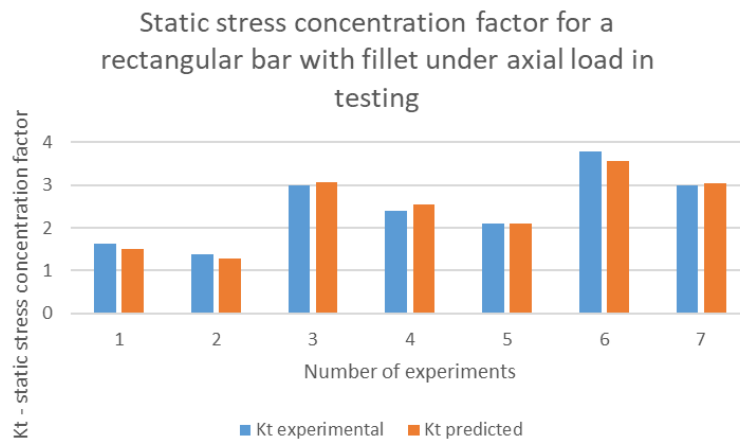


Fig. 9. Stress concentration factor K_t for a rectangular bar with fillet Under Axial Loading, in testing

Table 5. The weights and bias values for the ANN model proposed

The input-to-hidden layer weights	
W1	
0.0021	13.3296
0.321	-13.4838
-33.7648	-0.6031
6.1134	-0.8335

The hidden-to-output layer weights			
W2			
-291.208	-245.151	0.0527	-0.4038

The input-to-hidden layer bias
B1
-12.4989
3.3992
0.1677
5.6969

The hidden-to-output layer bias
B2
-46.6049

5. Conclusions

This study contains the determination of stress concentration factor using Peterson’s Stress Concentration Factor charts and formulas and ANN modelling. Peterson's graphs have been accepted as scientifically valid and so the Roark’s formula.

The values in these graphs can be defined only as a result of experimental studies. It is easier and more practical to determine these values using auxiliary software instead of using formulas.

A new ANN model was developed using Matlab software. Different ANN models were tried and the best model was determined.

The ANN model provided high accuracy for the prediction of stress concentration factor (K_t).

By using the ANN model, the user can avoid misreading the data in the charts.

The hierarchy of the two input variables assumes that the second variable D/d has a greater influence in determining the stress concentration factor than the r/d ratio.

Using weights and biases calculated, for r/d = 0.05 and D/d = 1.2 is obtained the stress concentration factor predicted $K_t = 2.0535$ (Table 6).

Table 6. Test for a pair of input variables that are not found in the training or testing data

r/d	D/d	K_t predicted
0.05	1.2	2.0535

References

[1]. **Boger Z., Guterman H.**, *Knowledge extraction from artificial neural network models*, IEEE Systems, Man, and Cybernetics Conference, Orlando, FL, USA, 1997.
 [2]. **Budynas-Nisbett**, *Shigley’s Mechanical Engineering Design*, 8th Edition.

[3]. **Haykin S.**, *Neural Network: A Comprehensive Foundation*, New York, Macmillan, 1994.
 [4]. **Abhishek K., Kishore D. J., Prakashkumar Kavalur, Akshay N. H.**, *ANN modeling for prediction of cutting force component during orthogonal turning*, International Research Journal of Engineering and Technology (IRJET), vol. 5, issue 6, June 2018.
 [5]. **Souâd Makhfi, Raphaël Velasco, Malek Habak, Kamel Haddouche, Pascal Vantomme.** *An Optimized ANN Approach for Cutting Forces Prediction in AISI 52100 Bearing Steel Hard Turning*, p-ISSN: 2163-2669, e-ISSN: 2163-2677, 3 (1), p. 24-32, doi: 10.5923/j.scit.20130301.03, 2013.
 [6]. **Maunayri H.**, *Novel Artificial Neural Networks Force Model for end Milling*, Springer, International Journal of Advanced Manufacturing Technology, 18, p. 693-700, 2001.
 [7]. **Krzysztof L. Molski**, *Stress concentration at load-carrying fillet welded cruciform joints subjected to tensile and bending loads*, Acta mechanica et automatica, vol. 13 no. 4, DOI 10.2478/ama-2019-0033, 2019.
 [8]. **Pilkey Walter D., Pilkey Deborah F.**, *Peterson’s stress Concentration Factors*, 3rd Edition.
 [9]. **Saurabh Karsoliya.** *Approximating Number of Hidden Layer neurons in Multiple Hidden Layer BPNN Architecture*, International Journal of Engineering Trends and Technology, vol. 3, issue 6, 2012.
 [10]. **Ihsan Toktas, Murat Tolga Ozkan, Fulya Erdemir, Nurullah Yuksel**, *Determination of Stress Concentration Factor (K_t) for a Crankshaft under Bending Loading: An Artificial Neural Networks Approach*, Politeknik Dergisi, Journal of Polytechnic, ISSN: 1302-0900 (PRINT), ISSN: 2147-9429 (ONLINE), 2020.
 [11]. **Alan J. Thomas, Miltos Petridis, Simon D. Walters, Saeed Malekshahi Gheytsi, Robert E. Morgan.** *On Predicting the Optimal Number of Hidden Nodes*, International Conference on Computational Science and Computational Intelligence, 2015.
 [12]. **Warren C. Young, Richard G. Budynas**, *Roark’s Formulas for Stress and Strain*, 8th Edition.
 [13]. ***, <https://mechanical.com/calculators/stress-concentration/>.
 [14]. ***, *MATLAB 2018a*, The MathWorks, Inc., Natick, Massachusetts, United States.

ANNEX A

Training data			
	$\frac{r}{d}$	$\frac{D}{d}$	K_t experimental
1	0.01	1	2
2	0.04	1	1.49
3	0.05	1	1.47
4	0.09	1	1.3
5	0.01	1.5	4.8
6	0.02	1.5	3.5
7	0.04	1.5	2.8
8	0.06	1.5	2.15
9	0.07	1.5	2.1
10	0.08	1.5	2
11	0.09	1.5	1.98
12	0.01	2	5.4
13	0.02	2	4.3
14	0.04	2	3.4
15	0.06	2	2.8
16	0.07	2	2.6
17	0.08	2	2.5
18	0.09	2	2.3

Testing data			
	$\frac{r}{d}$	$\frac{D}{d}$	K_t experimental
1	0.025	1	1.625
2	0.075	1	1.375
3	0.03	1.5	3
4	0.05	1.5	2.4
5	0.07	1.5	2.1
5	0.03	2	3.8
7	0.05	2	3

DETERMINATION OF STRESS CONCENTRATION FACTOR FOR A STEPPED BAR UNDER BENDING LOADING: AN ARTIFICIAL NEURAL NETWORKS APPROACH

Doina BOAZU

Department of Mechanical Engineering, "Dunarea de Jos" University of Galati, Romania
e-mail: doina.boazu@ugal.ro

ABSTRACT

Even today, charts and formulas derived from experimental determinations are used to obtain the stress concentration factor.

Stress concentration factors from charts can be converted into numerical values using computational techniques. Stress concentration factor values were collected in a database and an Artificial Neural Network (ANN) model can be developed for improving the database. ANN model provides accuracy in obtaining the stress concentration factors. Using the static stress concentration factor for a stepped bar under a bending load we can quantify the impact of notches in fatigue.

KEYWORDS: Stress Concentration Factor (SCF), Artificial Neural Network (ANN), bending loading

1. Introduction

The main objective of this paper is to develop an ANN model to properly predict the stress concentration factor (K_t) for a stepped bar under bending loading.

Stress concentration factor K_t can be obtained experimentally (especially using photo-elasticity), analytically and published in charts taking into account geometric property. This stress concentration factor is very important in brittle materials. For ductile materials the stress concentration factor is important in fatigue calculation when the safety is critical in the localized yielding hardens material.

In recent years, numerical models have been developed based on experimentally validated data using analytical formulas or by simulation using FEM; these models are obtained using simple regression, ANN approach or FEM simulation with optimization module.

The numerical finite element simulation is often time-consuming but an ANN model can predict with good accuracy the stress concentration factor while reducing the required time for the analysis [16].

Toktas [16], developed an ANN model with high accuracy for the prediction of stress concentration factor (K_t), for a Crankshaft under Bending Loading.

Stress concentration factor K_t is used in determining the fatigue concentration factor K_f .

2. Experimental background

Most structures that are designed have features such as holes, fillets and other notch shapes that cause stress concentration. Fatigue cracks commonly occur at these notches because at this location stresses are highest. An obstruction in a flow field of stresses increases the stresses around the obstruction. Notch is a general term meaning any or all of the fillets, holes, etc. The amount of stress around a notch is:

$$\sigma_{max} = K_t \cdot \sigma_{nom} \quad (1)$$

The stress concentration factor K_t provides the amplification of the stress at a notch relative to a nominal stress σ_{nom} . K_t is usually determined using charts or formulas [10].

The value of σ_{max} computed above is used when evaluating static failure due to yielding by the theory (von Mises) or the maximum shear stress criterion (Tresca) or when evaluating brittle static failure.

When evaluating the effect of notches on the fatigue resistance of a machine part, we use the fatigue stress concentration factor K_f instead of the stress concentration factor K_t . The fatigue stress concentration factor is usually smaller than the stress concentration factor.

The stress concentration factor in fatigue is [19]:

$$K_f = 1 + q(K_t - 1) \quad (2)$$

We use the notch sensitivity factor q to quantify the influence of notches in fatigue [20]:

$$q = \frac{1}{1 + \frac{\sqrt{a}}{\sqrt{r}}} \quad (3)$$

where \sqrt{a} is Neuber's constant and r is the notch size; Neuber's constant depends on the value of the ultimate tensile strength S_{ut} of the material used [9].

For bending and axial stress, the Neuber's constant can be calculated using the relation (for steel) [20]:

$$\sqrt{a} = 0.246 - 3.08(10^{-3})S_{ut} + 1.51(10^{-5})S_{ut}^2 - 2.67(10^{-8})S_{ut}^3$$

In practice, it is always safe to use K_t instead of K_f .

The elements that influence the stress concentration factor for a stepped bar in bending are represented in Fig. 1. The bar has an applied bending moment M . The parameters involved in the stress concentration factor K_t are (see Fig. 1):

- D = width of the larger section;
- d = width of the smaller section;
- r = radius of fillet;
- h = bar thickness;
- M = applied bending moment.

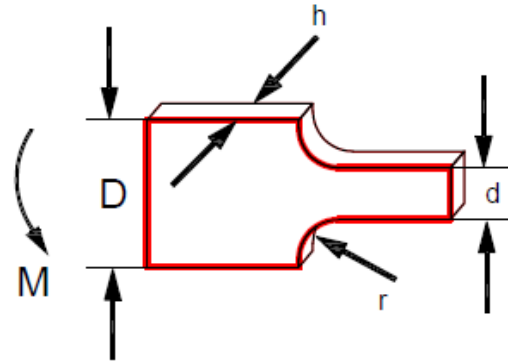


Fig. 1. Parameters involved in the calculation of the stress concentration factor for a stepped bar in bending [10, 20]

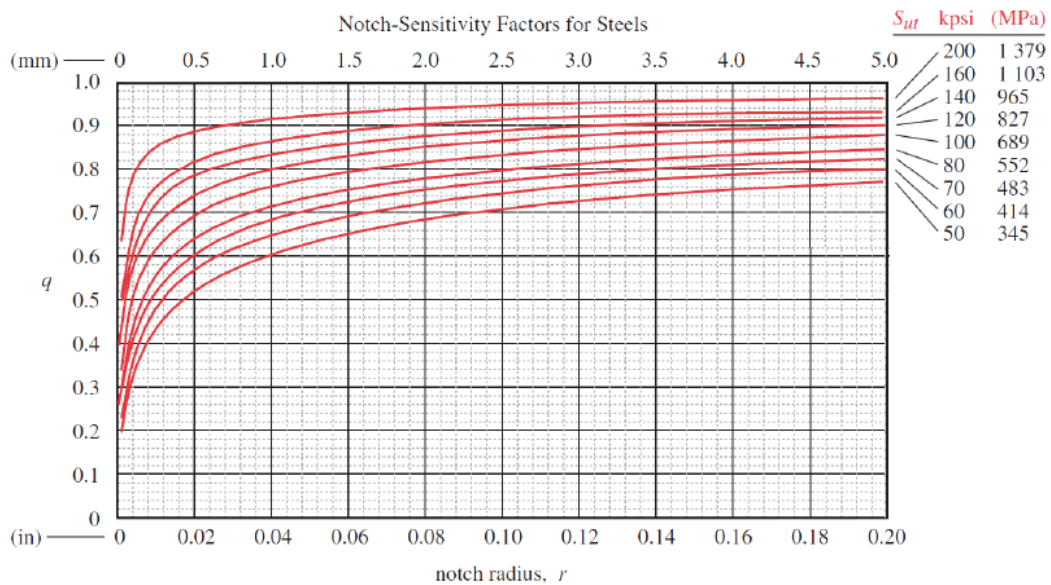


Fig. 2. Notch Sensitivity Curves for steel [13]

The stress concentration factor is calculated using formula 6 with coefficients from Table 1 [10].

$$\sigma_{nom} = 6 \frac{M}{h \cdot d^2} \quad (4)$$

$$\sigma_{max} = K_t \cdot \sigma_{nom} \quad (5)$$

$$K_t = A \left(\frac{r}{d} \right)^b \quad (6)$$

Table 1. Coefficients A and b as a function of D/d from relation (6)

D/d	A	b
3	0.90720	-0.0333
1.2	0.9959	-0.23829
1.01	0.96689	-0.15417

The stress concentration factors in fatigue is calculated using formula 2 with the notch sensitivity factor q from formula 3 and K_t from the formula 6. The notch sensitivity factor q can be obtained from Fig. 2 as a function of material (Steel) S_{ut} and the notch radius.

The training and the testing data (the experimental data) for stress concentration factor K_t in the case of a stepped bar in bending are given in the tables from Annex A.

3. Neural network modeling

Neural Network is a vast domain of technology where one can implement human brain modelling decisions into computer programs based on error and approximation.

The hierarchical network structure has an Input layer, an Output layer and between them a Hidden layer (Fig. 3).

In fitting problems, we want a neural network to map between a data set of numeric inputs and a set of numeric outputs (targets).

Training a neural network is used to perform a particular function by adjusting the values of the connections (weights + biases) between elements.

Neural networks are adjusted (by training) so that a particular input leads to a specific target.

The Input layer is a layer which communicates with the external environment and represents a pattern to the neural network. The Input layer should represent the condition for which we are training the neural network (Fig. 3).

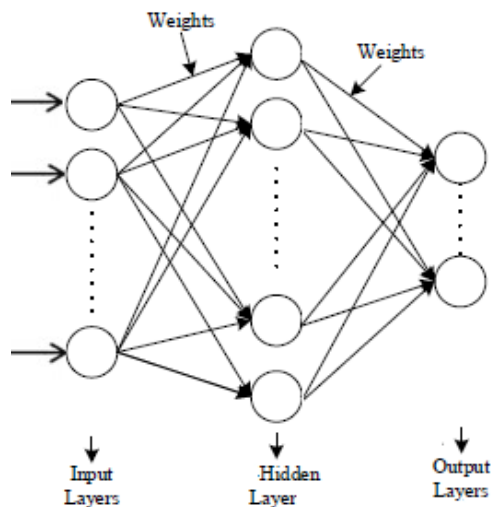


Fig. 3. ANN structure with one hidden layer [6]

The Output layer of the neural network represents a pattern to the external environment (Fig. 3).

The number of output neurons should be directly related to the type of work that the neural network is intended to achieve.

The Hidden layer is the collection of neurons which has an activation function applied to it. The Hidden layer provides an intermediate layer between the Input layer and the Output layer (Fig. 3).

The output response (s) using non-linear function is calculated as follows (eq. 7), [7]:

$$s = f(\sum w_i \cdot e + b) \quad (7)$$

During training, weights (w) and biases (b) are initialized to small random values to avoid sharp saturation in activation functions (f).

The main objective of this study is the development of an ANN model to properly predict the major element influence on the stress concentration factor for stepped bars in bending loading.

The input and output variables are dimensionless quantities and there is no need for their standardization to obtain a fast optimal Regression coefficient R .

Some major parameters used in the final ANN model have been optimized:

- the type of activation functions in hidden and output layers;
- the number of hidden layers;
- the number of neurons in the hidden layer.

Two activation functions need first to be chosen: one applied in hidden layers and the second used in the output layer to determine the appropriate number of hidden neurons and output values.

It is a good practice to use the Sigmoid function the $(f(x) = 1/(1 + e^{-x}))$ in hidden layer and the Linear function $(f(x) = x)$ in the output layer (S.L.) [7].

It is chosen a 2-4-1 ANN structure and the corresponding numerical model has been expressed on equation (8):

$$Output = f_k(b_k + \sum w_{kj} \cdot f_j(b_j + \sum w_{ji} \cdot x_i)) \quad (8)$$

Where w_{ji} and w_{kj} are respectively the weights that connect input i to hidden layer j and hidden layer j to output layer k , b are biases and f are activation functions.

It is recommended that the number of hidden layers is 1-5 [5, 16], but many times good results can be obtained with a single hidden layer and in this sense many tests are to be made [1]. In practice, one or two hidden layers are sufficient to solve any nonlinear complex problem [1].

All experiments were carried out using the MATLAB R2014b neural network toolbox [18].

The Levenberg-Marquardt (LM) learning algorithm version was used at the training and testing stages of the Networks.

The input and output variables are dimensionless quantities and without any standardization, we can obtain a fast optimal Regression coefficient R.

The regression coefficients for training different ANN structures and performance from Table 1 are highlighted in Fig. 4, Fig. 5, Fig. 6a; performance in training for the ANN structure 2-4-1 is given in the Fig. 6b.

The data from Table 2 highlights that the ANN-selected model is one with a single hidden layer with 4 neurons.

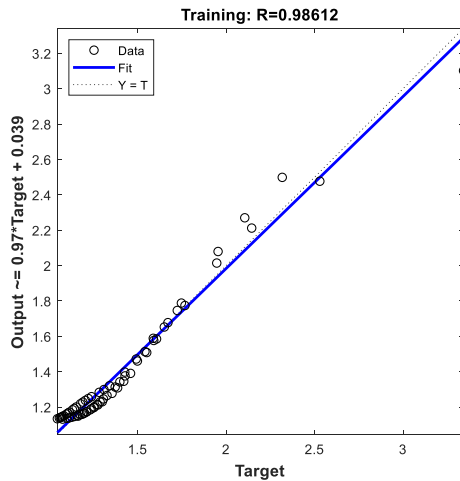


Fig. 4. ANN structure 2-2-1 R training

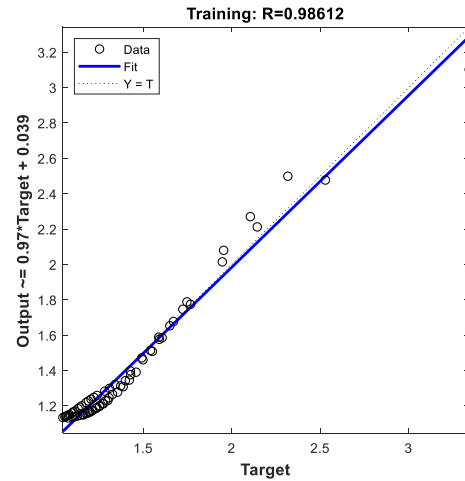


Fig. 5. ANN structure 2-3-1 R training

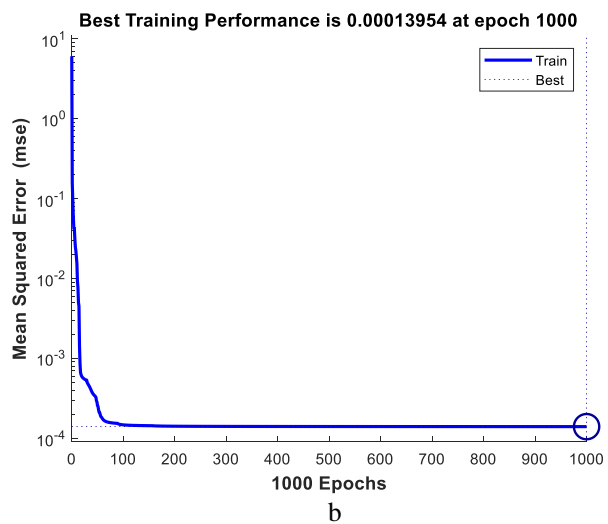
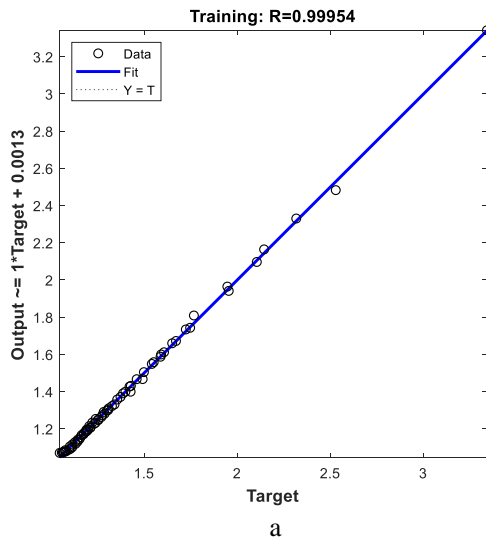


Fig. 6. a - ANN structure 2-4-1 R training; b - ANN structure 2-4-1 Performance in training

Table 2. R-training with performance in training and in testing

ANN structure	R- training	Performance in training	Performance in testing
2-2-1	0.98612	0.0041	0.0037
2-3-1	0.99391	0.0018	0.0029
2-4-1	0.99954	1.3954e-4	2.7565e-4

Three coefficients are calculated to evaluate statistical network performance: linear regression coefficient R, RMSE and MAPE [18] (Table 2).

The root mean square error (RMSE):

$$RMSE = \sqrt{\frac{\sum_{i=1}^n \|y_i - \hat{y}_i\|^2}{n}}$$

The mean absolute percentage error (MAPE):

$$MAPE = \frac{1}{n} \sum_{i=1}^n \left| \frac{\hat{y}_i - y_i}{y_i} \right| \times 100 \%$$

For linear regression coefficient R we used formula:

$$R = \frac{\sum_{i=1}^n (y_i - \bar{y})(\hat{y}_i - \bar{\hat{y}})}{\sqrt{\sum_{i=1}^n (y_i - \bar{y})^2 \cdot (\hat{y}_i - \bar{\hat{y}})^2}}$$

Where n is the number of experiments, y_i is the actual value, \hat{y}_i is the predicted value, \bar{y} and $\bar{\hat{y}}$ are mean target and predicted output values.

The coefficients calculated to evaluate the statistical network performance of the ANN model for a stepped bar in bending (Table 2) show the numerical model accuracy.

Table 2. Statistical Performance of training ANN model

Linear regression coefficient	Root Mean Square Error (RMSE)	Mean absolute percentage error (MAPE) %
0.99954	0.0118	0.58

4. Prediction of stress concentration factor

The Levenberg-Marquardt (LM) optimization algorithm has been used all along this study, in order to find out weights and biases.

The proposed ANN model has a single hidden layer with 4 neurons (Fig. 7).

Stress concentration factors K_t from experimental and predicted for training and testing data are given in the Table 3 and respectively in Table 4.

The graphic representation of the comparison between the experimental results and the predicted ones highlights the accuracy of the ANN model (Fig. 8 and Fig. 9).

The weights and biases values for the ANN model proposed are given in Table 5; with weights and biases thus determined and taking into account

the formula (8) values of the stress concentration factor K_t for a stepped bar in bending can be obtained for input data in the field in which the training was carried out.

Weights and biases values are given in Table 5.

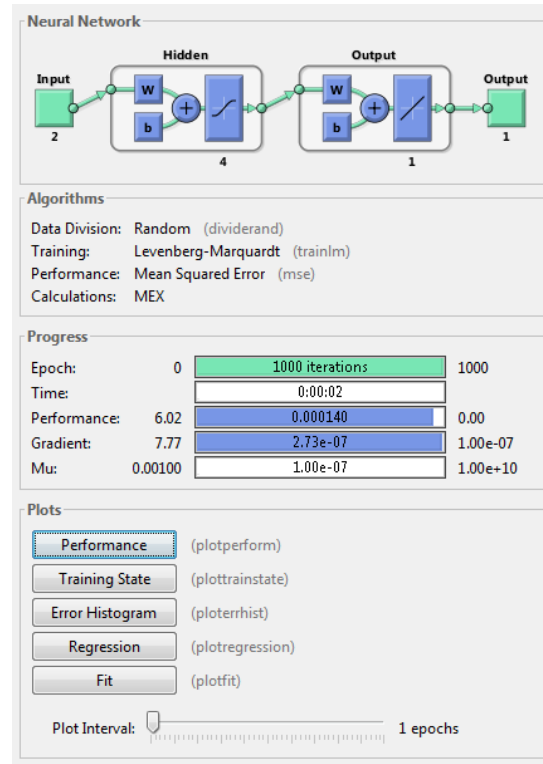


Fig. 7. ANN model using MATLAB

Table 3. Stress concentration factor K_t experimental and predicted for training data

Training data			
r/d	D/d	K_t experimental	K_t predicted
0.02	1.01	1.767288	1.8089
0.04	1.01	1.588172	1.5873
0.06	1.01	1.491934	1.4669
0.08	1.01	1.427209	1.3992
0.12	1.01	1.340725	1.3309
0.14	1.01	1.309238	1.3095
0.16	1.01	1.282561	1.2904
0.2	1.01	1.239188	1.2528
0.22	1.01	1.221113	1.2335
0.24	1.01	1.204841	1.2141
0.26	1.01	1.190065	1.195
0.28	1.01	1.176545	1.1768
0.32	1.01	1.152572	1.1444

Training data			
r/d	D/d	K_t experimental	K_t predicted
0.34	1.01	1.14185	1.1308
0.36	1.01	1.131832	1.1191
0.4	1.01	1.113596	1.1008
0.42	1.01	1.105251	1.094
0.44	1.01	1.097352	1.0885
0.48	1.01	1.08273	1.0805
0.5	1.01	1.075937	1.0776
0.52	1.01	1.069451	1.0754
0.54	1.01	1.063246	1.0736
0.56	1.01	1.057302	1.0723
0.6	1.01	1.046115	1.0703
0.02	1.2	2.529667	2.4828
0.04	1.2	2.144524	2.1642
0.06	1.2	1.947018	1.9644
0.1	1.2	1.723875	1.7339
0.12	1.2	1.650584	1.6597
0.14	1.2	1.591054	1.5994
0.16	1.2	1.541225	1.5485
0.18	1.2	1.498569	1.5043
0.22	1.2	1.428597	1.4305
0.24	1.2	1.399282	1.3992
0.26	1.2	1.372846	1.3709
0.3	1.2	1.326822	1.3218
0.32	1.2	1.306573	1.3005
0.34	1.2	1.287833	1.2811
0.36	1.2	1.270411	1.2633
0.38	1.2	1.254149	1.2471
0.4	1.2	1.238913	1.2322
0.44	1.2	1.211093	1.2062
0.46	1.2	1.198332	1.1948
0.48	1.2	1.186241	1.1843
0.52	1.2	1.163829	1.1659
0.02	3	3.34211	3.3421
0.06	3	2.317298	2.3302
0.08	3	2.105407	2.0967
0.1	3	1.954488	1.9411
0.14	3	1.747126	1.7428
0.16	3	1.671066	1.672
0.18	3	1.606731	1.6113

Training data			
r/d	D/d	K_t experimental	K_t predicted
0.2	3	1.551282	1.5578
0.24	3	1.459813	1.4664
0.26	3	1.421379	1.4268
0.28	3	1.386698	1.3905
0.3	3	1.355171	1.3572
0.34	3	1.299796	1.2984
0.36	3	1.275266	1.2726
0.38	3	1.252489	1.2488
0.4	3	1.231256	1.2269
0.42	3	1.211394	1.2068
0.44	3	1.192754	1.1882
0.46	3	1.175211	1.1712
0.48	3	1.158657	1.1555
0.5	3	1.142998	1.1411
0.52	3	1.128152	1.1278
0.54	3	1.114049	1.1156
0.56	3	1.100625	1.1044
0.6	3	1.075603	1.0846

Table 4. Stress concentration factor K_t experimental and predicted for testing data

Testing data			
r/d	D/d	K_t experimental	K_t predicted
0.1	1.01	1.378945	1.3584
0.18	1.01	1.259481	1.2717
0.3	1.01	1.164097	1.1598
0.38	1.01	1.122437	1.1091
0.46	1.01	1.089857	1.084
0.58	1.01	1.051597	1.0712
0.08	1.2	1.818019	1.8304
0.2	1.2	1.461414	1.4654
0.28	1.2	1.348815	1.3452
0.42	1.2	1.224593	1.2186
0.5	1.2	1.174757	1.1747
0.04	3	2.65264	2.7057
0.12	3	1.839245	1.8293
0.22	3	1.502773	1.5099
0.32	3	1.326329	1.3266
0.58	3	1.087826	1.0941

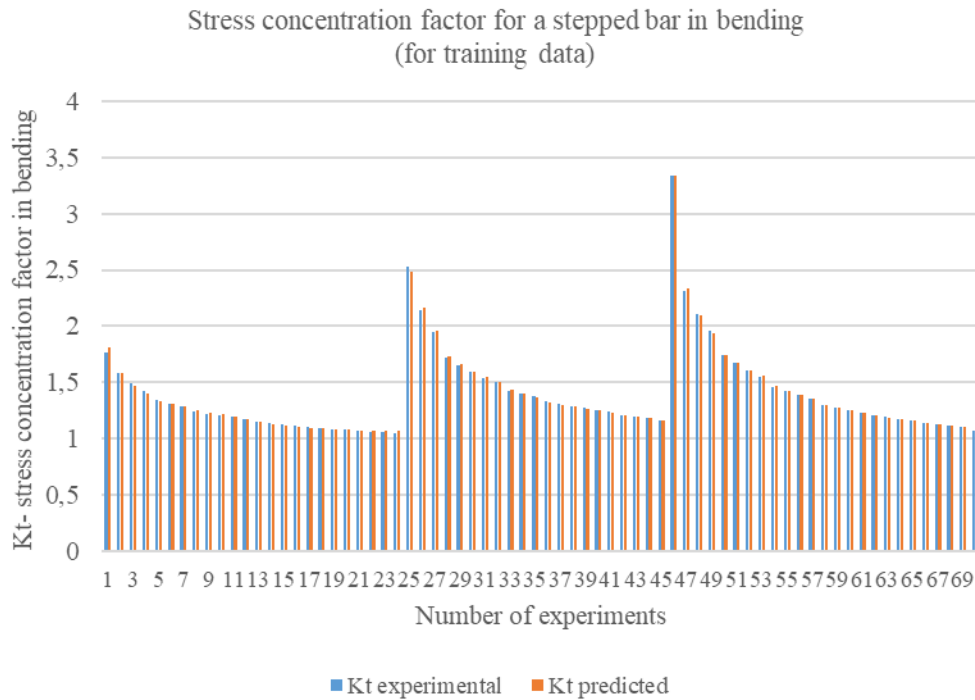


Fig. 8. Stress concentration factor K_t for a stepped flat bar in bending (for training data)

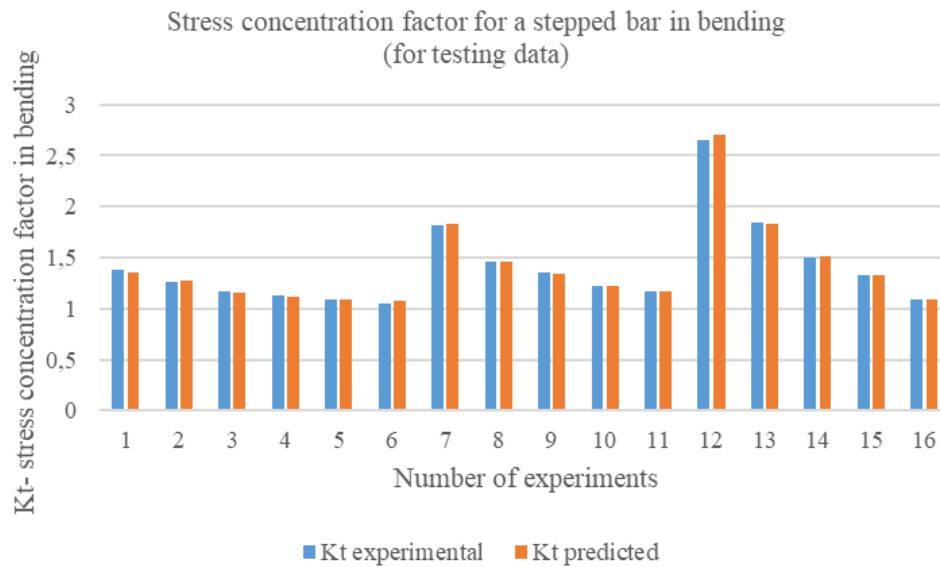


Fig. 9. Stress concentration factor K_t for a stepped flat bar in bending (for testing data)

Table 5. The weights and bias values for the proposed ANN model

the input-to-hidden layer weights	
W1	
0.6064	7.5884
0.6169	-27.0678
-1.8291	-9.137
4.6657	-0.231

the hidden-to-output layer weights			
W2			
-59.6062	-59.5662	0.1319	-38.2879

the input-to-hidden layer bias
B1
-4.6275
-18.7273
-9.6117
7.0611

the hidden-to-output layer bias
B2
37.3983

5. Conclusions

This study contains the stress concentration factor for the stepped bar in bending position, obtained using formulas from [10] and an ANN approach.

The formula for the stress concentration factor was defined only with the result of experimental studies. It is easier and more practical to determine these values using auxiliary software instead of using formulas.

A new ANN model was developed using Matlab software. Different ANN models were tried and the best model was obtained.

The ANN model provided high accuracy for the prediction of stress concentration factor (K_t) - see Table 2 with Statistical Performance of training ANN model.

Users may misread the values from the charts. By using the ANN model these faults were eliminated.

Using weights and biases of the ANN model, for $r/d = 0.045$ and $D/d = 2$ one obtained the stress concentration factor predicted $K_t = 3.2801$ (see Table 6).

Table 6. Test for a pair of input variables that are not found in the training or testing data

r/d	D/d	K_t predicted
0.045	2	3.2801

References

[1]. **Boger Z., Guterman H.**, *Knowledge extraction from artificial neural network models*, IEEE Systems, Man, and Cybernetics Conference, Orlando, FL, USA, 1997.
 [2]. **Budynas-Nisbett**, *Shigley's Mechanical Engineering Design*, 8th Ed.

[3]. **Giannini F., Laveglia V., Rossi A., Zanca D., Zugarini A.**, *Neural Networks for Beginners A fast implementation in Matlab*, Torch, TensorFlow, March 17, 2017.
 [4]. **Simon Haykin**, *Neural Networks and Learning Machine*, Third Edition, Pearson Prentice Hall, 2009.
 [5]. **Saurabh Karsoliya**, *Approximating Number of Hidden layer neurons in Multiple Hidden Layer BPNN Architecture*, International Journal of Engineering Trends and Technology – vol. 3, issue 6, 2012.
 [6]. **Abhishek K., Kishore D. J., Prakashkumar Kavalur, Akshay N H.**, *ANN modeling for prediction of cutting force component during orthogonal turning*, International Research Journal of Engineering and Technology (IRJET), vol. 5, issue 6, June, 2018.
 [7]. **Souâd Makhfi, Raphaël Velasco, Malek Habak, Kamel Haddouche, Pascal Vantomme**, *An Optimized ANN Approach for Cutting Forces Prediction in AISI 52100 Bearing Steel Hard Turning*, p-ISSN: 2163-2669, e-ISSN: 2163-2677, 3(1), p. 24-32, doi: 10.5923/j.scit.20130301.03, 2013.
 [8]. **Krzysztof L. Molski**, *Stress concentration at load-carrying fillet welded cruciform joints subjected to tensile and bending loads*, Acta mechanica et automatica, vol. 13, no. 4, DOI 10.2478/ama-2019-0033, 2019.
 [9]. **Neuber H.**, *Theory of Stress Concentration for Shear-Strained Prismatical Bodies with Arbitrary Nonlinear Stress-Strain Law*, ASME Journal of Applied Mechanics, 28, 1961.
 [10]. **Robert Norton**, *Machine Design – An integrated Approach*, 6th Edition, Pearson Publisher, 2014.
 [11]. **Foram S. Panchal, Mahesh Panchal**, *Review on Methods of Selecting Number of Hidden Nodes in Artificial Neural Network*, International Journal of Computer Science and Mobile Computing, vol. 3, issue 11, p. 455-464, November 2014.
 [12]. **Peterson R. E.**, *Stress concentration factors*, John Wiley and Sons, 1975.
 [13]. **George Sines, Waisman J. L.**, *Metal Fatigue*, McGraw-Hill Book Company, 1959.
 [14]. **Alan J. Thomas, Miltos Petridis, Simon D. Walters, Saeed Malekshahi Gheytsi, Robert E. Morgan**, *On Predicting the Optimal Number of Hidden Nodes*, International Conference on Computational Science and Computational Intelligence, 2015.
 [15]. **Alan J. Thomas, Simon D. Walters, Saeed Malekshahi Gheytsi, Robert E. Morgan, Miltos Petridis**, *On the Optimal Node Ratio between Hidden Layers: A Probabilistic Study*, International Journal of Machine Learning and Computing, vol. 6, no. 5, October 2016.
 [16]. **Ihsan Toktas, Murat Tolga Ozkan, Fulya Erdemir, Nurullah Yuksel**, *Determination of Stress Concentration Factor (K_t) for a Crankshaft under Bending Loading: An Artificial Neural Networks Approach*, Politeknik Dergisi, Journal of Polytechnic, ISSN: 1302-0900 (PRINT), ISSN: 2147-9429 (ONLINE).
 [17]. **Pilkey Walter D., Pilkey Deborah F.**, *Peterson's Stress Concentration Factors*, 3rd Edition.

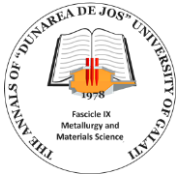
[18]. ***, Matlab, The MathWorks, Inc., Natick, Massachusetts, United States, 2018a.
 [19]. ***, <https://materion.com/-/media/files/alloy/newsletters/technical-tidbits/issue-no-60---effect-of-stress-concentration-on-fatigue-life.pdf>.

[20]. ***, <https://users.wpi.edu/~cfurlong/me3320/lect14/Lect14.pdf>.
 [21]. ***, https://research.iaun.ac.ir/pd/jjfesharaki/pdfs/UploadFile_9038.pdf.

ANNEX A

Training data		
r/d	D/d	K_t experimental
1	2	3
0.02	1.01	1.767288
0.04	1.01	1.588172
0.06	1.01	1.491934
0.08	1.01	1.427209
0.12	1.01	1.340725
0.14	1.01	1.309238
0.16	1.01	1.282561
0.2	1.01	1.239188
0.22	1.01	1.221113
0.24	1.01	1.204841
0.26	1.01	1.190065
0.28	1.01	1.176545
0.32	1.01	1.152572
0.34	1.01	1.14185
0.36	1.01	1.131832
0.4	1.01	1.113596
0.42	1.01	1.105251
0.44	1.01	1.097352
0.48	1.01	1.08273
0.5	1.01	1.075937
0.52	1.01	1.069451
0.54	1.01	1.063246
0.56	1.01	1.057302
0.6	1.01	1.046115
0.02	1.2	2.529667
0.04	1.2	2.144524
0.06	1.2	1.947018
0.1	1.2	1.723875
0.12	1.2	1.650584
0.14	1.2	1.591054
0.16	1.2	1.541225
0.18	1.2	1.498569
0.22	1.2	1.428597

0.24	1.2	1.399282
0.26	1.2	1.372846
0.3	1.2	1.326822
0.32	1.2	1.306573
0.34	1.2	1.287833
0.36	1.2	1.270411
0.38	1.2	1.254149
0.4	1.2	1.238913
0.44	1.2	1.211093
0.46	1.2	1.198332
0.48	1.2	1.186241
0.52	1.2	1.163829
0.02	3	3.34211
0.06	3	2.317298
0.08	3	2.105407
0.1	3	1.954488
0.14	3	1.747126
0.16	3	1.671066
0.18	3	1.606731
0.2	3	1.551282
0.24	3	1.459813
0.26	3	1.421379
0.28	3	1.386698
0.3	3	1.355171
0.34	3	1.299796
0.36	3	1.275266
0.38	3	1.252489
0.4	3	1.231256
0.42	3	1.211394
0.44	3	1.192754
0.46	3	1.175211
0.48	3	1.158657
0.5	3	1.142998
0.52	3	1.128152
0.54	3	1.114049
0.56	3	1.100625
0.6	3	1.075603



Testing data		
r/d	D/d	K_t experimental
1	2	3
0.1	1.01	1.378945
0.18	1.01	1.259481
0.3	1.01	1.164097
0.38	1.01	1.122437
0.46	1.01	1.089857
0.58	1.01	1.051597
0.08	1.2	1.818019

0.2	1.2	1.461414
0.28	1.2	1.348815
0.42	1.2	1.224593
0.5	1.2	1.174757
0.04	3	2.65264
0.12	3	1.839245
0.22	3	1.502773
0.32	3	1.326329
0.58	3	1.087826

CHALLENGES IN INTEGRATING GREEN BUILDINGS INTO EVERYDAY LIFE

Simona STANCA

Technical University of Cluj-Napoca, Buildings and Management Department, Romania
e-mail: simona.stanca@ccm.utcluj.ro

ABSTRACT

In recent decades, problems related to climate change, pollution and resource depletion have become increasingly urgent. Green architecture, also known as green buildings or sustainable construction, is an innovative response to these challenges. In this paper, the concept of green buildings, their benefits, and main characteristics, as well as their role in promoting a sustainable future for architecture and the environment will be explored.

Integrating the green buildings into everyday life is an important challenge, but also an extremely necessary one in the context of climate change and concern for environmental sustainability. Green buildings are structures designed to be more environmentally friendly and generate less impact on natural resources. Despite their obvious benefits, however, there are some significant challenges that need to be overcome to promote their integration into everyday life.

While these challenges exist, efforts to integrate green buildings into everyday life are still essential to ensure a more sustainable and greener future for future generations. Over time, as technology advances, awareness grows, and regulations improve, these challenges are expected to be overcome and green buildings to become a regular part of the urban landscape.

KEYWORDS: green buildings, sustainability, environment, quality of life

1. Introduction

In recent decades, an increasingly present theme in urban development is sustainability. An innovative and promising approach to achieving this goal is green or green buildings. In essence, the green buildings are designed and constructed in such a way as to minimize negative environmental impacts and provide significant social and economic benefits. From improving air quality to resource efficiency, these structures are becoming increasingly popular in major cities around the world.

The green buildings are thought of from a holistic perspective, considering all aspects, from design and construction to operation and demolition [2].

The green building concept is based on four fundamental principles: efficiency, utility, durability, and comfort. By following these four principles, green buildings contribute to protecting the environment, saving resources, and improving the quality of life of occupants and the communities in which they are located (Fig. 1) [5].



Fig. 1. Fundamental principles for green buildings [5]

2. Materials and technologies recommended and used in green buildings

Green buildings, also known as green or sustainable buildings, are constructions designed to be energy efficient and environmentally friendly. These buildings use a variety of specific materials and technologies to reduce environmental impact and promote sustainable resource use [1].

Here are some materials and technologies recommended and used in green buildings:

- Effective thermal insulation: Materials such as polyurethane foam, mineral wool, cellulose, and mineral wool can reduce heating and cooling requirements, thereby minimizing energy consumption (Fig. 2) [9].



Fig. 2. Insulating materials [9]

- Geothermal systems use natural energy thermal from the earth for heating and cooling, being a sustainable and energy-efficient option (Fig. 3) [19].



Fig. 3. Geothermal heat pumps [19]

- Solar panels and photovoltaic cells: Green buildings can be equipped with solar panels to generate electricity or hot water. PV cell technology can be integrated into roofs, windows, or walls to maximize energy efficiency (Fig. 4) [12].

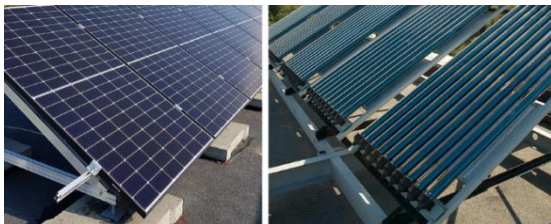


Fig. 4. Solar panels and photovoltaic cells [12]

- Green roofs: The systems green roofs involve planting vegetation on building roofs, which helps reduce district heating, improve air quality, and manage stormwater (Fig. 5) [11].



Fig. 5. Green roofs [11]

- Rainwater collection systems: These systems collect rainwater for use in irrigation, toilets, and other non-drinking needs, thus helping to save water (Fig. 6) [4].

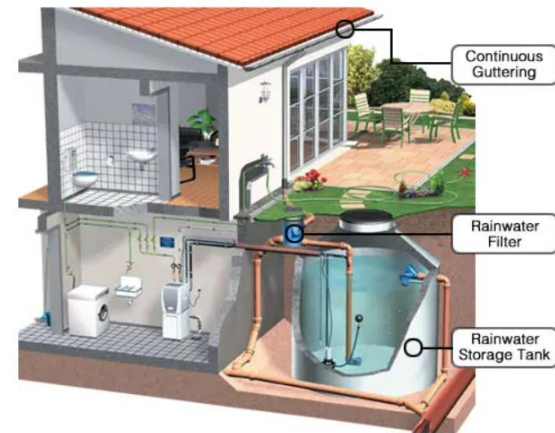


Fig. 6. Rainwater collection system [4]

- Recycled and renewable materials: Using recycled materials, such as recycled wood or metal, and renewable materials, such as bamboo or hemp, help reduce environmental impact [2].

- Efficient lighting systems: Use LED lights or other energy-efficient lighting systems help reduce electricity consumption (Fig. 7) [18].



Fig. 7. Efficient lighting systems [18]

- Natural ventilation: Building design allow adequate natural ventilation reduces the need for air-conditioning systems.

- Use of low-emission materials chemicals: The green buildings seek to use materials with low emissions of volatile chemicals (VOCs) to ensure better indoor air quality.

- Green certifications: green buildings can seek to obtain green certifications such as LEED (Leadership in Energy and Environmental Design) or BREEAM (Building Research Establishment Environmental Assessment Method) certifications to demonstrate commitment to sustainability and environmental performance.

These are just a few examples of materials and technologies used in the green buildings. The field of sustainable construction is constantly evolving, and research and innovation continue to bring new solutions and options for environmentally friendly buildings.

3. Challenges and opportunities

The integration of the green buildings in everyday life brings challenges, but also remarkable opportunities for protecting the environment, improving the quality of life, and promoting sustainable development.

Challenges regarding the integration of green buildings in everyday life:

- High initial costs: In general, building a green building may involve higher upfront costs than traditional buildings. Higher upfront investments can discourage developers from adopting sustainable solutions, even if they prove to be more economical and energy efficient in the long run.

- Public awareness and education: The integration of green buildings requires increased public awareness of the importance of protecting the environment and the benefits of sustainable buildings. Education in this direction can lead people to support and demand the development of the green buildings.

- Inappropriate regulations and policies: Laws and Building regulations are not always environmentally friendly enough, which can make it difficult for green buildings to develop. Government policies must support and stimulate the adoption of sustainable construction practices.

- Resistance to change: In many cases, building developers and owners may be resistant to adopting new technologies and methods needed to transform traditional buildings into green buildings. It may be caused by lack of information or knowledge to make such changes.

- Implementing new technologies: Integration green buildings often involve the use of innovative technologies and materials, which can be difficult to

obtain or implement, especially in regions with limited resources.

- Life cycle of buildings: It is important to ensure that the green buildings are durable and can withstand time. Proper management of the building, as well as of the materials and techniques used in its construction, are essential to ensure that sustainable benefits are realized in the long term.

- Energy efficiency: green buildings must be designed to be more energy efficient, but sometimes there may be difficulties in achieving this goal due to the structural restrictions or high costs of green technologies.

- Urban influence: Integrating green buildings in the urban context may involve adjusting infrastructure, transport, and other aspects of cities, which can be logistically and financially challenging.

Opportunities for integrating green buildings into everyday life:

- Positive impact on the environment: Buildings Green can contribute significantly to reducing the carbon footprint, conserving energy, and sustainably using natural resources.

- Long-term savings: Although costs Can initially be higher, green buildings offer significant energy and maintenance savings in the long term, leading to increased financial efficiency.

- Improving Quality of Life: Using Eco-friendly materials and smart design can improve indoor air quality, providing a healthier working and living environment.

- Competitive advantages: Properties with Ecological certification can attract more customers and tenants, due to the growing concern for sustainability and environmental protection.

- Innovation and economic development: The development and deployment of green technologies can generate new business opportunities and jobs in sustainability.

- Attraction for investors: Investing in Green buildings can become more attractive to investors as they reflect an environmentally oriented vision for the future.

- Health benefits: Using Energy efficiency, as well as the use of environmentally friendly materials, can help reduce indoor pollution and thus improve the health of green building occupants.

- Encouraging technological innovation: The development of green buildings stimulates research and innovation in sustainable technologies, having a positive impact on society.

Overcoming challenges requires a collaborative effort between developers, governments, research institutions and the community to implement policies and support measures that encourage and facilitate the development of these buildings.

4. Advantages and disadvantages of green buildings

Advantages of green buildings:

- **Energy efficiency:** green buildings use energy-efficient systems and technologies such as solar panels, superior thermal insulation, geothermal, LEDs, sensor lighting systems, etc. This leads to significant savings on utility bills.
- **Resource efficiency:** Buildings Greens reduce water consumption and use sustainable and recyclable materials, which reduces the impact on natural resources.
- **Indoor Air Quality:** The Design and the materials used in green buildings help reduce toxic emissions and improve indoor air quality, leading to a healthier environment for occupants.
- **Low effect on the environment:** Green building has less impact on the environment as it reduces carbon emissions and helps protect ecosystems.
- **Certifications and recognition:** Green buildings can earn special certifications and recognition, such as LEED (Leadership in Energy and Environmental Design), which can enhance property value and bring tax benefits.

Disadvantages of green buildings:

- **Higher upfront costs:** Construction and the design of green buildings can involve higher costs compared to traditional buildings. The initial investment can be a disadvantage for developers or owners with limited budgets.
- **New Technology and Materials:** Implementation Eco-friendly technologies and materials may require additional learning and adaptation for architects, engineers, and builders.
- **Location limitations:** Some technologies greens may be more effective in certain geographies than others. Thus, some regions may find it difficult to adopt certain environmentally friendly solutions.
- **Maintenance and operating costs:** Some green technologies require special maintenance and, in some cases, higher operating costs in the long run.
- **Life cycle of materials:** Even if green buildings use recyclable and sustainable materials; their production and transport can still have a negative impact on the environment.

5. Notable examples of green buildings

Today, the green buildings are becoming increasingly popular in construction as they promote energy efficiency and environmental sustainability.

Here are some examples of green buildings:

- **The Edge - Amsterdam, Netherlands:** It was named "the smartest building in the world" due to its extensive use of IoT (Internet of Things) technology.

The building automatically adjusts its lighting, heating, and cooling system to ensure maximum energy efficiency (Fig. 8) [10].



Fig. 8. The Edge - Amsterdam, Netherlands [10]

- **One Angel Square - Manchester, Sea United Kingdom:** The headquarters of Co-operative Group is one of the most sustainable office buildings in the world. It has a double glass façade for thermal insulation and a cogeneration system that uses the energy produced for heating and cooling (Fig. 9) [15].

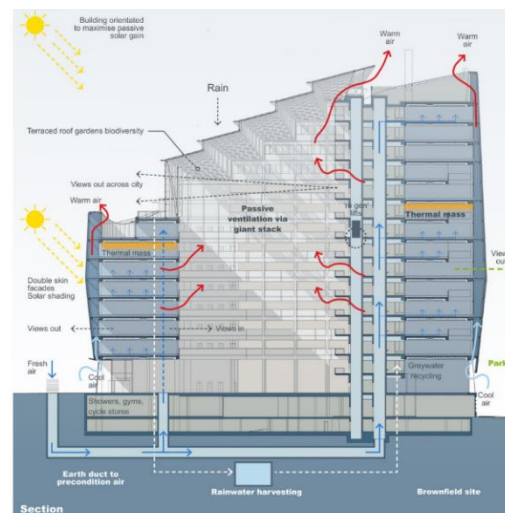


Fig. 9. One Angel Square - Manchester, Sea United Kingdom [15]

- Pixel Building - Melbourne, Australia: Australia's first office building with a maximum score of six Green Star stars. It has green roofs, rainwater collection systems and integrated solar panels for power generation (Fig. 10) [14].

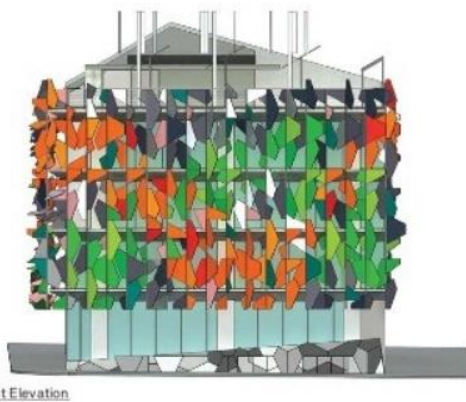


Fig. 10. Pixel Building - Melbourne, Australia [14]

- The Bullitt Center - Seattle, SUA: An outstanding example of a net-zero energy building using solar panels and advanced energy efficiency technologies. It focuses on environmentally friendly and sustainable materials (Fig. 11) [16].

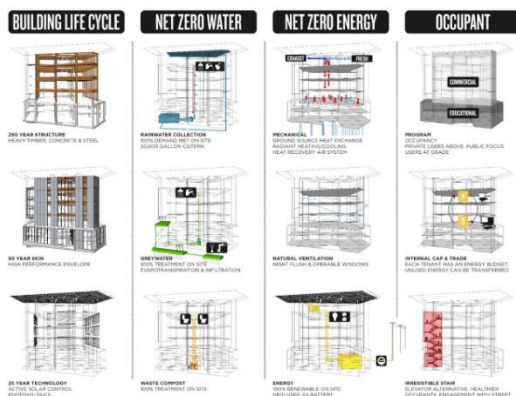


Fig. 11. The Bullitt Center - Seattle, SUA [16]

- Bahrain World Trade Center - Manama, Bahrain: This is an impressive building with integrated wind turbines, which contribute to the partial production of the energy needed by the building (Fig. 12) [13].



Fig. 12. Bahrain World Trade Center – Manama, Bahrain [13]



- Stuttgart City Library – Stuttgart, Germany: It was designed with a glass façade and natural ventilation system to maximize natural light and reduce electricity consumption (Fig. 13) [17].



Fig. 13. Stuttgart City Library – Stuttgart, Germany [17]

- The Crystal - London, United Kingdom: A sustainability centre showcasing innovative technologies and solutions to make cities more sustainable. The building itself is an example of eco-friendly and energy-efficient design. (Fig. 14) [6].



Fig. 14. The Crystal - London, United Kingdom [6]

In Romania, there is a significant increase in interest in the construction and certification of green buildings. These are some examples of notable green buildings in the country:

- Crystal Tower – Bucharest, a building in Romania BREEAM Certified at excellent level (Fig. 15) [7, 8].



Fig. 15. Crystal Tower – Bucharest [7, 8]

- residential complex WINGS Cluj Napoca: the first EDGE certified project in Romania (Fig. 16) [20].



Fig. 16. Residential complex WINGS Cluj Napoca [20]

- Residential complex SEASONS in Cluj Napoca: a spectacular concept of urban vertical forest (Fig. 17) [20].



Fig. 17. Residential complex SEASONS Cluj Napoca [20]

- City Business Centre, Timisoara: CBC is designed to ensure maximum comfort, efficiency, and access to all utilities (Fig. 18) [21].



Fig. 18. City Business Centre, Timisoara [21]

The green building industry continues to develop and grow as concern for the environment and energy efficiency becomes an increasing priority.

6. Conclusions

Integrating green buildings into everyday life is an important but necessary challenge for sustainable urban development [3]. Through awareness, education, proper regulation and collaboration between the public and private sectors, these challenges can be overcome. Finally, green buildings can make a significant difference in quality of life and environmental protection, making our cities greener, healthier, and more resilient to climate change.

References

- [1]. **Stanca S.**, *Refurbishment of Decommissioned Buildings in the Context of Sustainable Development*, Bul. Inst. Polit. Iași, 62 (66), 1, p. 61-71, ISSN: 1224-3884 (p), ISSN: 2068-4762 (e), 2016.
[2]. **Stanca S.**, *The Potential of Reconverting Functions for Buildings in Romania*, Bul. Inst. Polit. din Iasi, 64 (68), 3, p. 83-90. ISSN: 1224-3884(p), ISSN: 2068-4762 (e), Fascicolul 3, 2018.

- [3]. **Stanca S.**, Sustainability in construction, The Annals of "Dunarea de Jos" University of Galati Fascicle IX Metallurgy and Materials Science, ISSN 2668-4748 (Print), 2668-4756 (Online) Journal volume & issue, vol. 46, no. 1 p. 10-15, 2023.
[4]. ***, <https://casepractice.ro/colectarea-apei-de-ploaie/>, accessed in 3.07.2023.
[5]. ***, <https://despre-energie.ro/cum-sa-gandesti-o-cladire-verde-pentru-a-obtine-certificare-internationala/>, accessed in 3.07.2023.
[6]. ***, <https://effisus.com/en/effisusportfolio/europe/the-crystal-london/>, accessed in 6.07.2023.
[7]. ***, https://green-report.ro/romania-are-65-de-cladiri-verzi/?gclid=Cj0KCQjwk96IBhDHARIsAEKO4xalYr4sZYmobC7eb7Eo-2JqZpjz0G0Uxgev-sMOGCWFiMTOB-Lh5gaAssQEALw_wcB, accessed in 7.07.2023.
[8]. ***, <https://instalfocus.ro/top-5-cele-mai-verzi-cladiri-din-romania/>, accessed in 7.07.2023.
[9]. ***, <https://isoterm.ro/noutati/izolatie-termica-cum-izolam-eficient-si-ce-materiale-alegem/>, accessed in 12.07.2023.
[10]. ***, <https://plparchitecture.com/the-edge/>, accessed in 12.07.2023.
[11]. ***, <https://proiect-casa.ro/acoperis-verde-avantaje-deza-avantaje/>, accessed in 12.07.2023.
[12]. ***, <https://servelect.ro/panouri-fotovoltaice-vs-panouri-solare-termice-ce-alegem>, accessed in 12.07.2023.
[13]. ***, <https://www.arch2o.com/bahrain-world-trade-center-kill-design-arch2o-bahrain-world-trade-center-kill-design-12>, accessed in 14.07.2023.
[14]. ***, <https://www.archdaily.com/190779/pixel-studio505/5016faf728ba0d235b0007c0-pixel-studio505-phot>, accessed in 14.07.2023.
[15]. ***, <https://www.archdaily.com/337430/1-angel-square-3d-reid/512e54ccb3fc4bd78b00027b-1-angel-square-3d-reid-section>, accessed in 14.07.2023.
[16]. ***, <https://www.archdaily.com/363007/the-world-s-greenest-commercial-building-opens-in-seattle-today/5161f2d6b3fc4bc526000245-the-world-s-greenest-commercial-building-opens-in-seattle-today-photo>, accessed in 14.07.2023.
[17]. ***, <https://www.architectural-review.com/today/stuttgart-city-library-by-yi-architects>, accessed in 17.07.2023.
[18]. ***, <https://www.eorion.ro/blog/corpuri-de-iluminat-cu-led-eficienta-energetica>, accessed in 17.07.2023.
[19]. ***, <https://www.idm-energie.at/ro/terra/>, accessed in 20.07.2023.
[20]. ***, <https://www.studiumgreen.ro/seasons-ro/>, accessed in 20.07.2023.
[21]. ***, <https://www.uar-bna.ro/2016/proiecte/165/>, accessed in 20.07.2023.

COMPARATIVE STUDY REGARDING THE DESIGN OF A 3D PRINTED HIP PROSTHESIS

Silvia-Iuliana NECULA, Vasile BAŞLIU, Vasile BRIA, Marius BODOR*

"Dunarea de Jos" University of Galati, Romania
*e-mail: marius.bodor@ugal.ro

ABSTRACT

This work proposes the comparison of two models of 3D printed hip prostheses, using microscopic and chemical analysis, but also compression and bending testing. The comparison was made using a hip prosthesis designed in the Autodesk Inventor 2020 program and a model freely available on the Internet. The work includes some details about the virtual prototyping of prostheses and results from the chemical analysis of the components of the hip prostheses, carried out using an X-ray spectrometer to identify the elements contained in the PETG (polyethylene terephthalate glycol) material that was used to obtain the samples. The second method of analysis was the microscopic one and finally the samples were subjected to external forces, through bending and compression testing. This comparison aimed to demonstrate the dependence between the shape of the prosthesis and the mechanical properties of the analysed samples.

KEYWORDS: virtual design, PETG, 3D printing, XRF, optical microscopy, mechanical testing

1. Introduction

Using the technology created in recent years, researchers working in the field of biotechnology, together with doctors in the field of orthopaedics, form research groups to improve artificial implants to better meet the needs of the patients. Recently, people tend to have more orthopaedic procedures such as total hip replacement at a young age. For this reason, researchers are constantly looking for ways to optimize endoprostheses either geometrically or from the point of view of the materials used in manufacturing, in order to reduce the number of postoperative revisions required by the patient and thus increase the life span [1].

Due to the technological advances made in recent years and especially due to the growth of the additive manufacturing industry, researchers are using virtual prototyping to take the patient's femoral mould directly from the film (tomography), trying to customize the design of the hip prosthesis. In this sense, the trend is towards using software that allows the user to select the size of anatomical landmarks and then generate the shape of the implant from algorithms. Finally, the resulting design can be manufactured using additive manufacturing (AM).

Additionally, recent studies of materials used in endoprosthesis manufacture attempt to regenerate bone tissue to reproduce a material that exhibits the same mechanical properties and properties as human bone tissue [2].

A femoral hip prosthesis is made of special alloys, such as titanium, to ensure the best biocompatibility. They are usually coated with hydroxyapatite to facilitate the growth of bone tissue on the prosthetic surface, resulting in better integration and complete fixation of the crown. Alternatively, the prosthesis can be cemented (typically used in patients with poor bone quality, such as elderly patients with bone demineralization) or cementless (typically used in young or active patients) [3].

The total hip prosthesis consists of three elements connected together, usually by pressing, designed to form a spherical contact that allows flexion, extension, shape, external rotation and internal rotation movements of the hip. The hip prosthesis and the surgical approach are based on the particularities of the hip morphology and the patient's medical history. Therefore, surgeons look for the best standard prosthesis for each patient and the most suitable medical treatment [4].

A 3D printing process always starts with the creation of a 3D digital model, which is the basis of the printed product [5]. Compared to traditional manufacturing options, 3D printing can turn a design into reality in just a few hours. There are also projects that require more time, but when it comes to small or medium volumes, 3D printing is definitely a much faster solution [6]. Additive manufacturing makes it easier to create new and innovative designs than traditional manufacturing processes. The very narrow angle limitations that require special tools in 3D printing are eliminated due to layers that can be easily overlapped regardless of shape [7]. 3D printing also has limitations, although significantly fewer than other processes. One of them is that 3D printed parts become weaker due to layering. Another limitation occurs with large volumes of 3D printed products, as production costs are significantly increased compared to other methods used. If the design on the printer is not well aligned, the 3D printed product may be inaccurate. CNC machines are sometimes used for precision finishing to increase the accuracy of the final product [8].

A variety of materials can be used in the 3D printing process. These include materials such as plastics, metals, ceramics and even concrete, but also less expected materials such as paper, edible materials and others [9]. They come in 3D filament, liquid resin or powder form and can be used in almost any type of 3D printer. Of course, the most commonly used are polymers and it is preferable to use specific materials for each technology [10]. The choice of material for 3D printing is very important and the success of the whole project depends on it [11].

For polymers, 3D printing offers many possibilities and can be used both for prototyping and for the creation of various landmarks and tools [12]. Materials from the polymer family include: Polyamide (PA 11) [12], Glass-filled Polyamide – used in techniques such as MJF (multi-jet fusion) in the manufacture of housings and closures [13], Polypropylene – used in techniques such as SLS (Selective Laser Sintering) and FFF/FDM (Fused Filament Manufacturing/Fused Deposition Modeling) in the production of food packaging and mechanical products that require low friction [14], Polycarbonate – Used to make supports or brackets in FFF/FDM [15], ABS – Used in FFF/FDM to create prototypes and devices [15].

Although the material used in this study is not a biocompatible one, the purpose of the work herein was satisfactorily met. This was done using two different types of designs for a hip prosthesis and the results of testing revealed the importance of this aspect when a decision comes into discussion. Results were obtained by using a virtual design environment to get the desired shape of the sample and then

printing this shape and a second one, based on another design. The samples were 3D printed using the same type of polymeric filament and the testing was done by using X-ray spectroscopy, optical microscopy and mechanical testing.

2. Materials and methods

To obtain the hip prostheses, a sketch is needed along with its dimensions. After analysing the sketch, the designing can start in the chosen program. In this case Autodesk Inventor 2020 was chosen. This program allows the creation, simulation and visualization of 3D products designed with professional engineering tools. It helps create a highly accurate virtual model to validate design form and function in real life, minimizing the need for testing using physical prototypes [16].

An Artillery Sidewinder X1 3D printer (Fig. 1) was used to fabricate the physical hip prostheses. Two prototypes were created using the additive manufacturing (AM) process, based on two models of the femoral prosthesis, the first model being made in the Inventor program and denoted P1, and the second model whose file was obtained online, denoted P2 (Fig. 2). AM-based 3D printing technology is one of the most widely used in the rapid prototyping process due to its affordable cost, equipment and high potential for printing a wide range of materials.

The material used in this process was polyethylene terephthalate glycol, known as PETG, a thermoplastic polyester with excellent chemical resistance, durability and moldability when manufactured, but not compatible with the human body [17].



Fig. 1. Presentation of the layout of the printer used to obtain the hip prostheses

After the stages in Autodesk Inventor for the design of the prosthesis, in the 2D and then in 3D, the next step towards printing the prosthesis was to enter the designed prosthesis in the Cura program. This program offers the possibility to choose the position

of printing the prosthesis, the height of the layer of the print, the thickness of the outer wall of the print and more. For the printing process, the printing temperature was chosen as 235 °C and the printing table temperature as 85 °C, for the layer height was chosen as 0.2 mm, for the initial layer height was

chosen as 0.32 mm and for the line width as 0.45 mm, the wall thickness and the number of wall lines, the wall thickness being 1.35 mm and the number of lines being 3, the filling density was chosen to be 40%, the filling line distance 1.125 mm and Gyroid was chosen as the filling pattern.



Fig. 2. The two models of hip prostheses: P1 – left; P2 – right

For chemical analysis an X-ray spectrometer, model INNOV-X SYSTEMS, α A-4000 was used. The samples were placed, one at a time, in front of the instrument's Kapton window and the data

acquisition (lasting for 30 seconds) was triggered from the instrument iPaq PDA, as presented in Figure 3.



Fig. 3. A hip prosthesis atop the X-ray spectrometer, model INNOV-X, α A-4000, during an X-ray analyses

The apparatus uses a standardless software based on fundamental parameter (FP) method. Fundamental parameter (FP) method is based on peak fitting for direct correlation of measured spectra and calculated element concentrations [18]. The apparatus returns the data to the user in the form of a graph represented as a function of energy between 0 – 40 [keV].

A KERN OLM 171 metallurgical microscope was used for the microscopic analysis, which belongs

to the series of inverted microscopes and has an ergonomic, robust and extremely stable design. The samples were not specially prepared for this type of analyses and the construction of the instrument made the manipulation of the sample very easy.

The Instron 8850 series system is a floor-model biaxial servo-hydraulic dynamic testing system that provides axial and torsional load on the specimen in an integrated biaxial actuator. With a precision-aligned two-column frame and high rigidity, the 8850

series meets the challenging requirements of a wide range of static and dynamic biaxial testing requirements [19]. This type of instrument was used for mechanical testing, bending and compression being the chosen possibilities.

For bending tests, the top support moved at 5 mm/min and the distance between the supports was

90 mm. To submit to external forces, the apparatus was turned on and the preparation of the test machine was awaited. After machine preparation, the P1 femoral stem was placed and bending was started. The same was done for the P2 femoral stem. Figure 4 presents the abovementioned architecture of the bending test.



Fig. 4. Bending test of P1 sample femoral stem – left and P2 sample femoral stem – right



Fig. 5. Compression test of P1 sample acetabular cup – left and P2 sample acetabular cup – right

For compression testing, two plates were used, one for support and the second for applying force. In this case the upper arm descended by 1.3 mm/min. For testing, the P1 acetabular cup was placed on the support plate and compression testing was started, after the testing of the first cup was completed, the testing of the P2 cup was started and then continued for all the other components: the liners of P1 and P2 samples and femoral heads of P1 and P2 samples.

3. Results and discussions

3.1. X-ray fluorescence analysis

Figure 6 presents the result of the XRF analysis of the P1 and P2 femoral stems. Visibly, there are no major differences between the results of the two

samples. With the help of the XRF spectrum provided by the device, it was possible to confirm the presence of chemical elements specific to the PETG material, namely: carbon, hydrogen, sulphur and oxygen. The specific energies of these elements are as follows for carbon $k\alpha = 0.28$ [keV], oxygen $k\alpha = 0.53$ [keV] and sulphur $k\alpha = 2.3$ [keV] [20]. As such from the XRF spectrum it is observed that the values are reduced and are found in the specific range of the background noise of the device.

This type of analyses emphasises the identical chemical composition of both samples used for comparison. This result was expected since the same material and parameters were used for both samples and the data only stands for confirmation of this expectation.

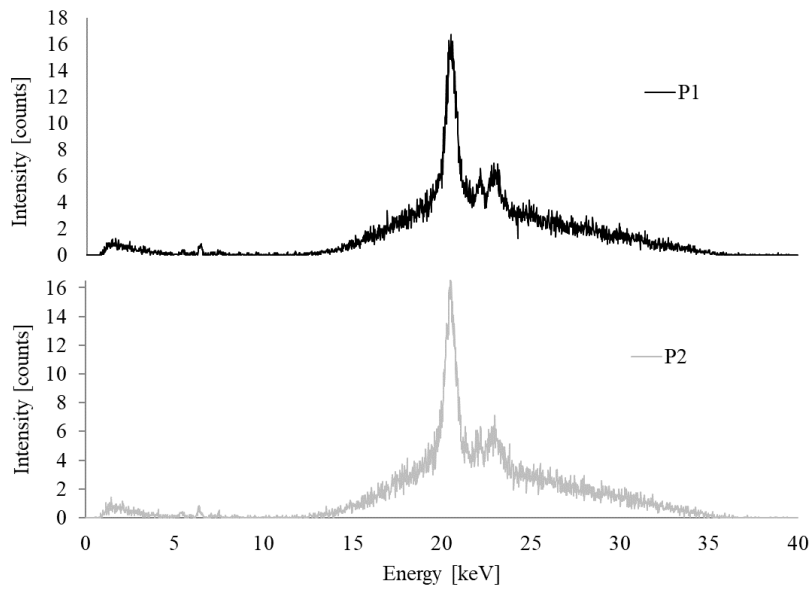


Fig. 6. Spectra obtained through X-ray fluorescence analyses of P1 and P2 sample femoral stems

3.2. Optical microscopy analysis

The obtained results were possible by using a 5x magnification, other magnifications being unfit to obtain proper images to compare the samples. The

purpose of this type of analysis is also to confirm the similarities between the two types of samples. All samples' components were analysed and compared as seen in Figures 7-10.

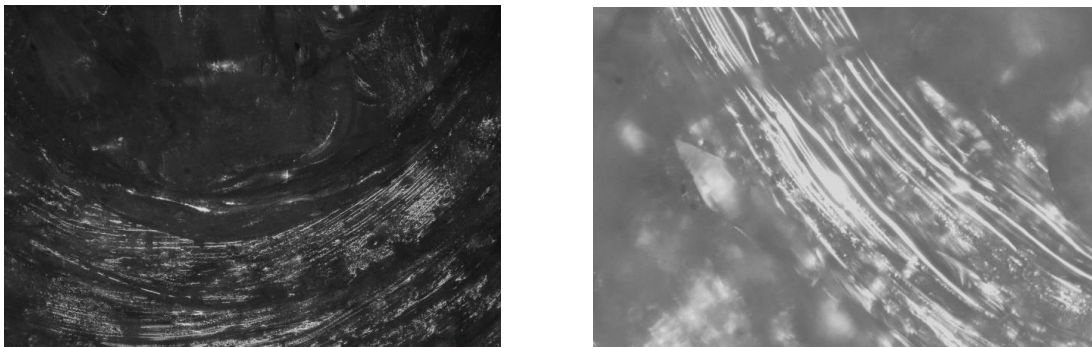


Fig. 7. Microscopic view at 5x magnification of P1 sample acetabular cup – left and P2 sample acetabular cup – right

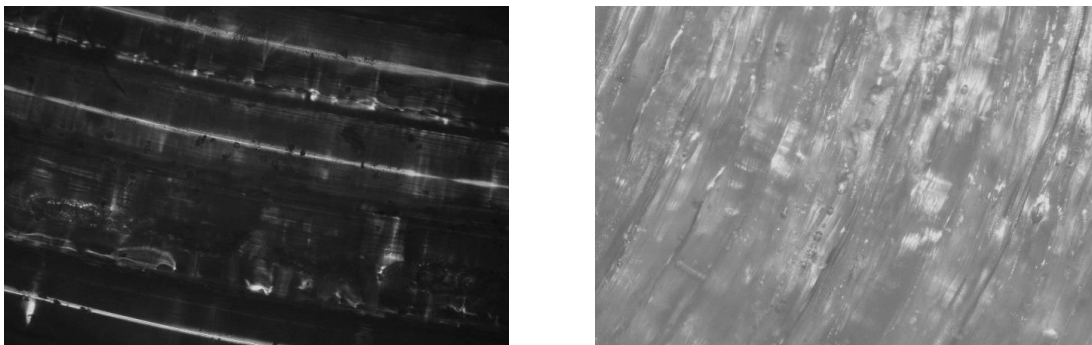


Fig. 8. Microscopic view at 5x magnification of P1 sample liner – left and P2 sample liner – right

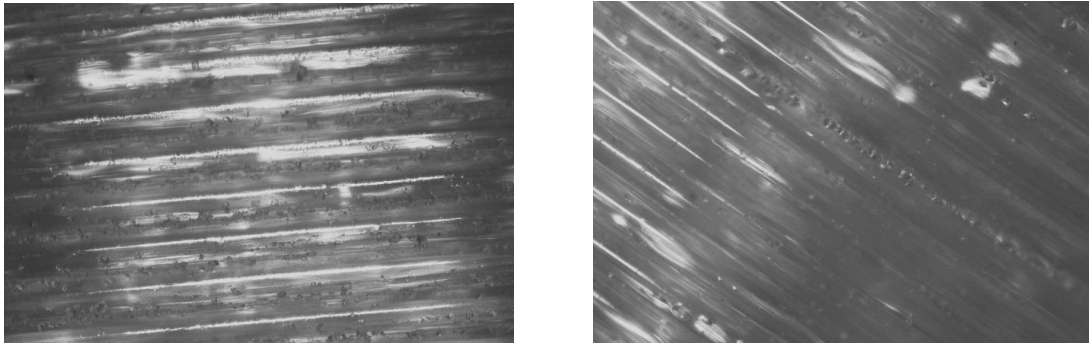


Fig. 9. Microscopic view at 5x magnification of P1 sample femoral head – left and P2 sample femoral head – right

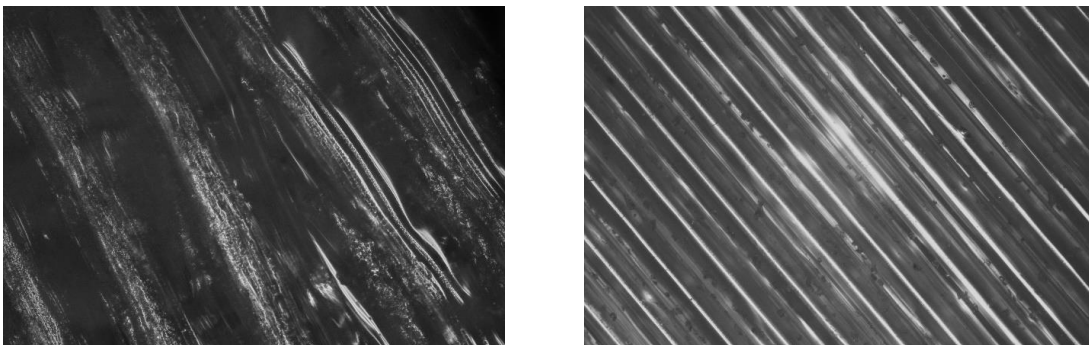


Fig. 10. Microscopic view at 5x magnification of P1 sample femoral stem – left and P2 sample femoral stem – right

Although the appearance of images for the same component of each sample was expected to be similar, some aspects may slightly differ due to the different angle during microscopic analysis. This is most noticeable in Figures 7 and 8, while the next two ones, Figures 9 and 10, present morphologies that look alike. Nevertheless, the morphological aspect of both samples also emphasises the common build-up that stands behind the two separate shapes used for comparison in this work.

3.3. Bending and compression testing

Using the mechanical testing device some results were obtained that finally differentiated one hip prosthesis design from the other. For this tests, first the femoral stem of P1 and P2 samples were tested from the bending point of view and then, all the other components were tested from the compression point of view and the data is presented in Figures 11-14.

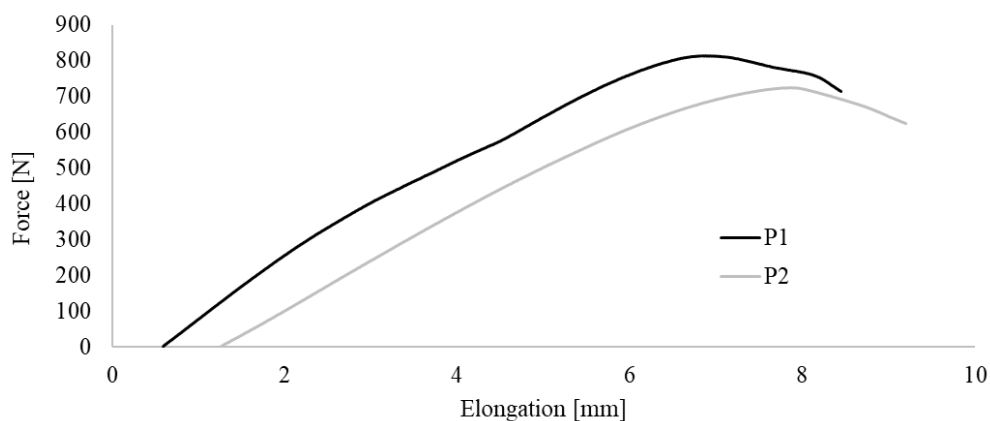


Fig. 11. Results of the bending test for P1 and P2 samples femoral stems

Figure 11 presents the results of the bending test. This type of testing was chosen since this type of stress is the most probable to be encountered for femoral stems and the data presented here emphasises a small difference in favour of the P1 sample femoral stem. The trends in elongation seem similar until around 700 N of applied force, although the elongation is constantly higher for P2 compared to P1. The automatic stop-point of the test is also very close for both samples from the force and elongation point of view, with the higher force value sustained

by P1, proving that this shape is more agreeable than the one of P2, when it comes to bending forces.

The next test, the compression of acetabular cups proved again in favour of P1 sample. Again, not too great, but observable differences are presented in Figure 12, this time the starting point being the same, as expected for this type of test. The higher stress sustained by P1 is observed throughout the testing time with lower strain, when compared to P2. Also, in this test, P2 sample acetabular cup sustained an abrupt rupture when reaching the highest stress.

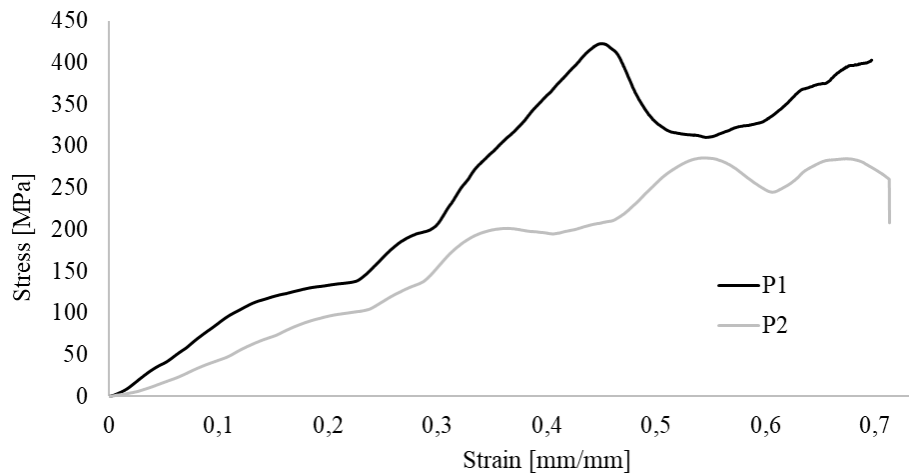


Fig. 12. Results of the compression test for P1 and P2 samples acetabular cups

When it comes for the comparison of data for the compression test of the liners, Figure 13 reveals an almost exact behaviour of the two tested objects, until approximately the value of 600 MPa of stress. Starting from this point, a slight difference is

observed in the behaviour during testing, this time in favour of the P2 sample liner, although only from the strain point of view, since the automatic stop-point value of the force is approximately the same, namely around 1400 MPa.

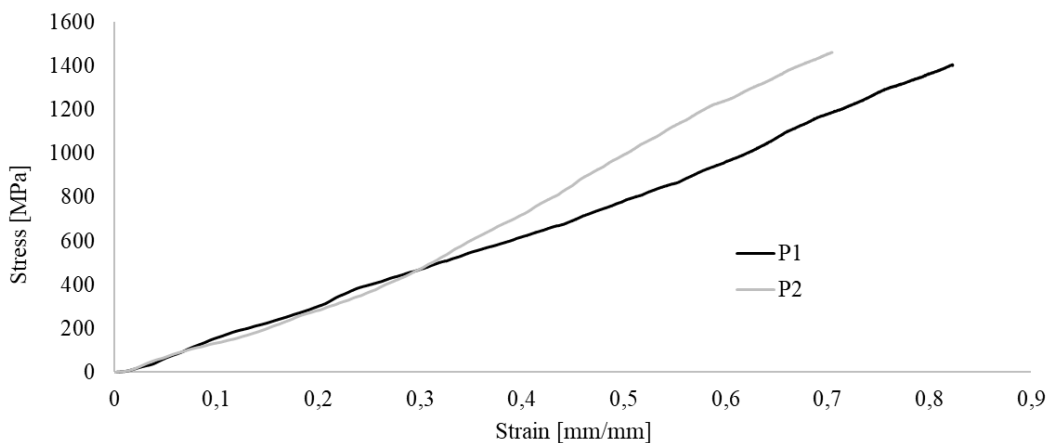


Fig. 13. Results of the compression test for P1 and P2 samples liners

Since the construction is almost the same, in case of the femoral heads the compression test offers almost the same data, the curves based on these data

being almost overlapped, as can be observed in Figure 14.

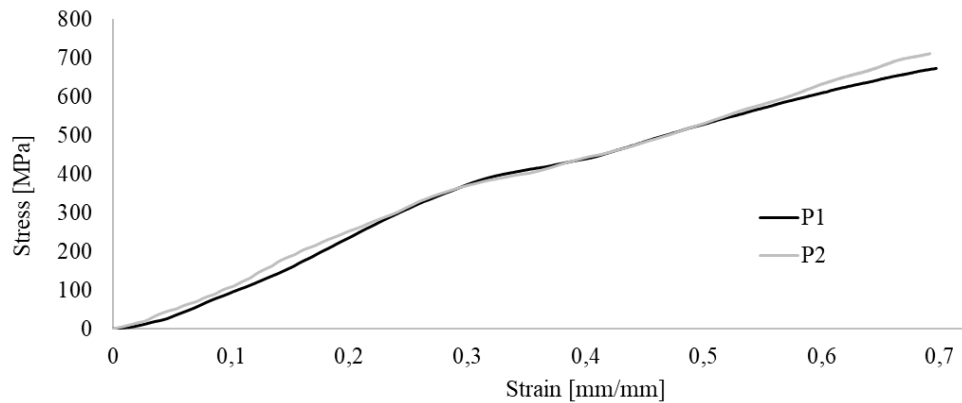


Fig. 14. Results of the compression test for P1 and P2 samples femoral heads

The results from the mechanical testing of all the components of the two femoral prosthesis, that were obtained in this work through 3D printing, demonstrates the advantage of the P1 sample design towards sustaining greater overall values of applied force and smaller deformation in contrast to the P2 sample design.

4. Conclusions

Virtual prototyping is now becoming increasingly important in the fields of biotechnology and medicine, as it provides the opportunity to analyse patient conditions, simulate various activities of daily life, and plan surgical interventions. The human body is an organic machine and although it has common characteristics when analysed in depth, there are many characteristics that make it unique both as an individual and as an organism and set it apart when discussing orthopaedic surgical approaches.

The obtained results demonstrate that both 3D printed prototypes were similar in chemical composition and structurally. Instead, mechanical testing demonstrated a clear, although small, advantage of the P1 hip prosthesis overall design in comparison to the P2 hip prosthesis design.

Future research directions could aim towards obtaining and testing different other designs of the hip prosthesis, using biocompatible materials.

References

[1]. ***, <https://www.romedic.ro/subiect/soldul>, accessed in 15.11.2022.

- [2]. ***, <http://grandhall.ro/9228-tratamentul-artrozei-fizice-actualului.php>, accessed in 15.11.2022.
- [3]. ***, https://www.researchgate.net/figure/Dispozitive-de-protezare-totala-a-articulațiilor-umane-a-Proteza-de-sold_fig1_264558595, accessed in 15.11.2022.
- [4]. ***, https://ugalromy.sharepoint.com/:w/g/personal/btudor_ugal_ro/ERyvmVd8KJ1En9QsgKhcRI0BMbe8v_AOMkDdRSfpdNaHhg?e=00Q8dH, accessed in 10.12.2022.
- [5]. ***, <https://www.zspotmedia.ro/blog/printare-3d/>, accessed in 10.01.2023.
- [6]. ***, <https://www.descopera.ro/stiinta/17838294-revolutie-in-tehnologia-imprimantelor-3d-cu-ajutorul-luminii-se-poate-printa-de-100-de-ori-mai-rapid>, accessed in 10.01.2023.
- [7]. ***, <https://3dminime.ro/media-si-referinte/>, accessed in 10.01.2023.
- [8]. ***, <https://www.firme365.ro/avantaje-si-dezavantaje-ale-printarii-3d-fabricarea-aditivata/>, accessed in 10.01.2023.
- [9]. ***, <https://www.simplify3d.com/>, accessed in 09.03.2023.
- [10]. ***, <https://www.materialise.com/en>, accessed in 12.04.2023.
- [11]. ***, <https://tusdswap.pw/634774-what-is-3d-printing-and-how-exactly-does-it-work>, accessed in 12.04.2023.
- [12]. ***, <https://jakevdp.github.io/PythonDataScienceHandbook/04.12-three-dimensional-plotting.html>, accessed in 12.04.2023.
- [13]. ***, https://journals.lww.com/prsgo/Fulltext/2023/04000/Three_dimensional_Medical_Printing_and_Associated.62.aspx, accessed in 12.04.2023.
- [14]. ***, <https://www.pcmag.com/news/3d-printing-what-you-need-to-know>, accessed in 12.04.2023.
- [15]. ***, <https://formlabs.com/blog/25-unexpected-3d-printing-use-cases/>, accessed in 12.04.2023.
- [16]. ***, <https://www.forscope.ro/autodesk-inventor/>, accessed in 23.04.2023.
- [17]. ***, <https://all3dp.com/1/artillery-sidewinder-x1-review-3d-printer-specs/>, accessed in 23.04.2023.
- [18]. ***, <https://www.bruker.com/en/products-and-solutions/elemental-analyzers/xrf-spectrometers/xrf-solutions/standardless-solutions.html>, accessed in 07.09.2023.
- [19]. ***, <https://www.instron.com/en/products/testing-systems/dynamic-and-fatigue-systems/8850-axial-torsion>, accessed in 29.04.2023.
- [20]. ***, http://ramontxrf.260mb.net/Periodic_Table_and_X-ray_Energies.pdf, accessed in 07.09.2023.

RECOVERY OF AGRICULTURAL WASTE TO OBTAIN COMPOST

Carmelia Mariana BĂLĂNICĂ DRAGOMIR

ORCID: 0000-0001-7743-928X

"Dunarea de Jos" University of Galati, Galati, Romania

e-mail: carmelia.dragomir@ugal.ro

ABSTRACT

The aim of this study is to make compost in a specialized container, using household and agricultural waste from own farm and the physicochemical characterization of obtained compost. The physicochemical characterization of the compost samples was carried out through the following determinations: determination of moisture, pH, determination of total soluble salts, determination of nitrate nitrogen, determination of nitrite, determination of ammonium nitrogen and determination of organic matter content. The compost samples analysed showed a high physicochemical quality. The use of compost offers environmentally friendly solutions with a long-term impact on the environment and quality of life.

KEYWORDS: compost, food waste, recycling

1. Introduction

Food waste can be transformed in many ways to produce different organic fertilizers and soil amendments. Conversion processes include composting, anaerobic digestion, dewatering, biochar production and chemical hydrolysis. Some food waste products can be used to remediate contaminated soils, in addition to improving soil properties [1].

Composting is the best method of recovery of organic residues and represents the totality of microbial, biochemical, chemical, and physical transformations that organic, vegetable and animal wastes undergo from their initial state until they reach different stages of humification, a state qualitatively different from the initial one, characteristic of the newly formed product, called compost [2]. Composting is an ancient form of recycling, long practiced by farmers to produce fertilizer material [3]. Compost is a complex of organic matter resulting from biomass waste: plant biomass, wood waste, sewage sludge waste, biodegraded by composting. In the composition of biodegradation products are present: carbohydrates from plant biomass structure, amino acids, simple lipids, fatty acids, carbohydrate end-biodegradation products, amino acid end-biodegradation, lipids, mineral compounds [4]. The chemical composition of the compost is influenced by the chemical composition of the composted materials, the ratio between these materials and the way the composting process was carried out [5].

The composting technique is one of the environmentally friendly waste conversion pathways as it returns part of the waste components to the environment. In Romania, composting in rural areas is done individually in households. Composting requires monitoring of parameters such as pH, oxygen content, particle size, temperature, time, bulk density, moisture, and C/N ratio to optimize its potential for use as a fertilizer [6].

Compost used as a soil fertilizer contributes to soil C fixation, fertility, biodiversity, soil physical properties by increasing erosion resistance and soil water uptake and retention capacity. The application of compost to soil is of considerable interest as a means of maintaining adequate soil structure and as a means of adding organic material to soil whose organic matter content has been reduced by intensive farming [7]. It is also used to remediate contaminated soils and for the slow release of nutrients from compost which is responsible for increasing crop yields in subsequent years. Due to the complex mechanisms by which compost has many benefits in the soil, it is necessary to take a brief look at soil structure and the correlations that are established between compost and soil [8]. Long-term use of compost for crop cultivation indicates that it has an equalizing effect on annual and seasonal fluctuations in soil water, air and heat balance, plant nutrient availability and therefore on final crop yields [9].

2. Materials and methods

The composting method consisted mainly of organizing composting platforms. At the bottom of the compost heap a 10-15 cm layer of thin branches and straw was formed to ensure drainage and aeration of the heap. The composting substrate consisted of

vegetable residues from the agricultural crops of corn, alfalfa, straw, leaves, grass and animal manure, which were mixed and moistened. The composting time was 6 months and samples were obtained in 2019, 2020, 2021. The block diagram on unit operations for composting is shown in Figure 1.

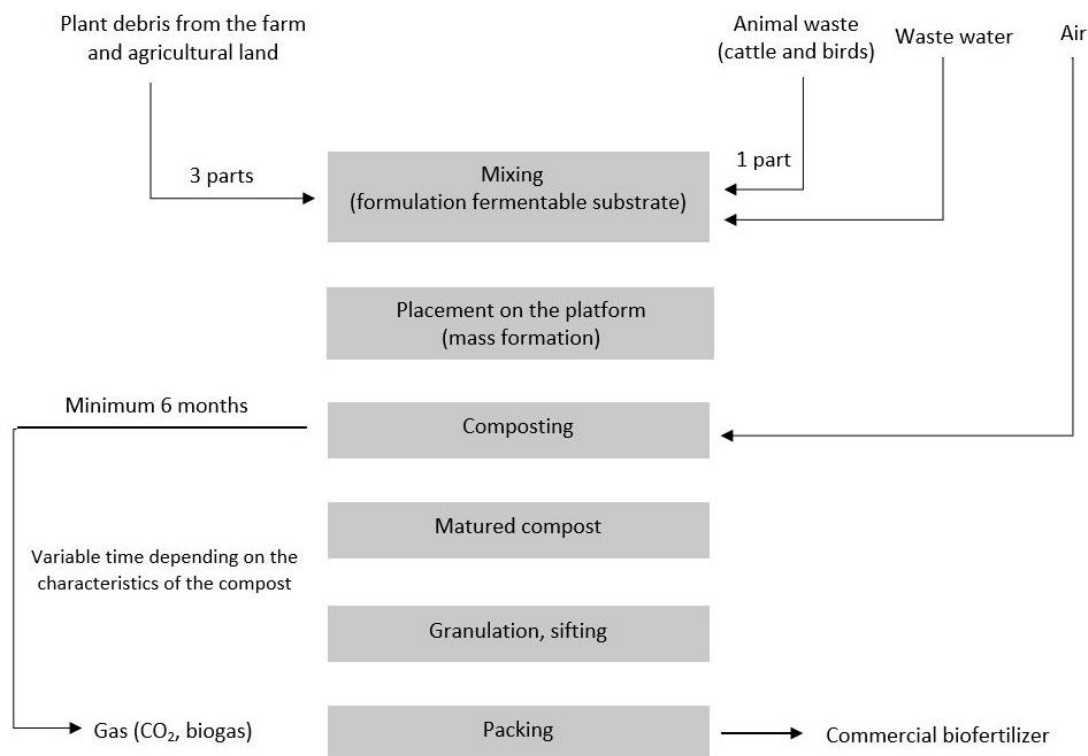


Fig. 1. The block diagram on unit operations for composting

2.1. Moisture determination

Compost moisture can be analysed on both freshly harvested and air-dried samples. The principle of the method is based on measuring the weight loss of a pre-air-dried sample after complete removal of water by drying at 105 °C, for 5-6 hours in the oven.

2.2. pH determination

The pH was measured using a Thermo Scientific Orion Star 4-pH meter.

2.3. Determination of total soluble salts content

Preparation of compost extract: distilled water was used to make the aqueous extract in order not to alter the solubility of some constituents in the

compost. 50 g of compost is added to a container with 250 mL CO₂-free distilled water. The suspension is stirred for 15 minutes using a stirrer and then filtered. The extract obtained is homogenized and used for the determination of total soluble salts and for the separate analysis of anions and cations.

The determination of the total amount of soluble salts in the compost was carried out by the conductometric method. The principle of the method is to measure the electrical conductivity of the aqueous compost extract obtained.

2.4. Nitrate-nitrogen determination

The extract was obtained by extracting nitric nitrogen with potassium sulphate solution. The nitrate-nitrogen determination was conducted by the colorimetric method using 2,4-phenoldisulfonic acid in alkaline conditions.

2.5. Nitrite determination

Nitrite analysis was performed by the colorimetric method using Griess reagent.

2.6. Determination of ammonia nitrogen

The principle of the method is based on the reaction between ammonium ions and Nessler reagent when yellow mercuric amidochloride iodide is formed. The intensity of the yellow colour is directly proportional to the concentration of ammonium ions in the extract analysed. The analysis is determined using a colorimetric method.

2.7. Determination of organic matter content in compost

The principle of the method is based on dry mineralization of organic matter by calcination at 800 °C.

3. Results and Discussion

3.1. Physicochemical characterization of compost

All the waste products used, in solid form (plant residues and droppings) from the farm were used as raw material for composting. Cattle manure used for composting, when mixed with bedding has particularly good composting qualities. Poultry droppings need to be mixed with carbon-rich

materials, preferably low nitrogen materials such as sawdust and straw. As substrates rich in carbon were used: wheat straw, corn cobs, bean and pea stalks, sunflower stalks, grass, and leaves. They were chopped to a size of 2-5 cm to obtain the best possible homogenization with the residual product, to ensure the largest possible contact surface and good aeration of the canopy. All the organic waste from the farm was deposited in the compost heap. A mixture was calculated to give an optimum moisture of 65%.

The compost samples showed a specific aspect, namely: the first sample had a black colour, loose structure, the second sample had a dark brown colour, slightly loosened structure, untransformed residues less than 20% and the third sample had a brown colour, compact structure, more than 20% transformed residues.

The results of the analysis of the compost samples obtained by evaluating moisture, pH, organic matter content, total soluble salts in the compost, nitrate nitrogen and ammonium nitrogen content are shown in the following Figures 2-9. All measurements were performed in duplicated, and the data presented represent the mean values of these replicates. The results were expressed as average values together with standard deviations. Statistical analysis of the data was conducted using Microsoft Excel.

Moisture values are slightly variable between samples and composting period and correlate with dry matter content. The results show that the pH has alkaline values, towards the upper limit of the standardized range. Following analysis, the dry matter was more than 50%, favourable result.

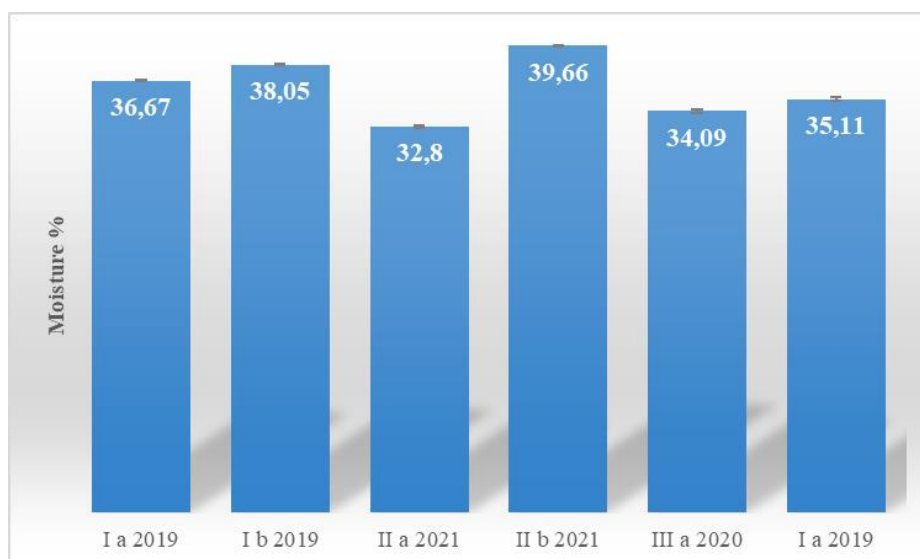


Fig. 2. Moisture variation of compost obtained in different time periods

A reduced number of soluble salts is observed in the compost samples obtained in 2019, due to the compositional variation of the composting substrate and composting conditions.

An exceptionally low content of organic matter in the compost is observed in the compost obtained in 2020. Samples I and III showed an organic matter content greater than 25%, favourable, the exception was sample II.

The samples analysed showed high values of nitrate content, but below 1 g/100 g dry compost, demonstrating the efficiency of the nitrification and denitrification steps. The lowest nitrate nitrogen values were observed in the 2021 samples. This is in direct correlation with the biochemical processes

taking place, especially the biotransformation steps of nitrogen compounds. Nitrite content had very low values, but higher than 0 as recommended. The results indicate that aeration of the pile is necessary. The ammonia nitrogen content was exceptionally low, and the nitrate nitrogen/total mineral ratio was greater than 0.5, a favourable result.

As can be noticed, the quality of the compost is variable from year to year and from barge to barge and is correlated with three categories of factors that have a particular impact on the biochemical processes, such as: substrate composition, microorganisms involved in biotransformation and the intrinsic and extrinsic physicochemical conditions of the composting environment.

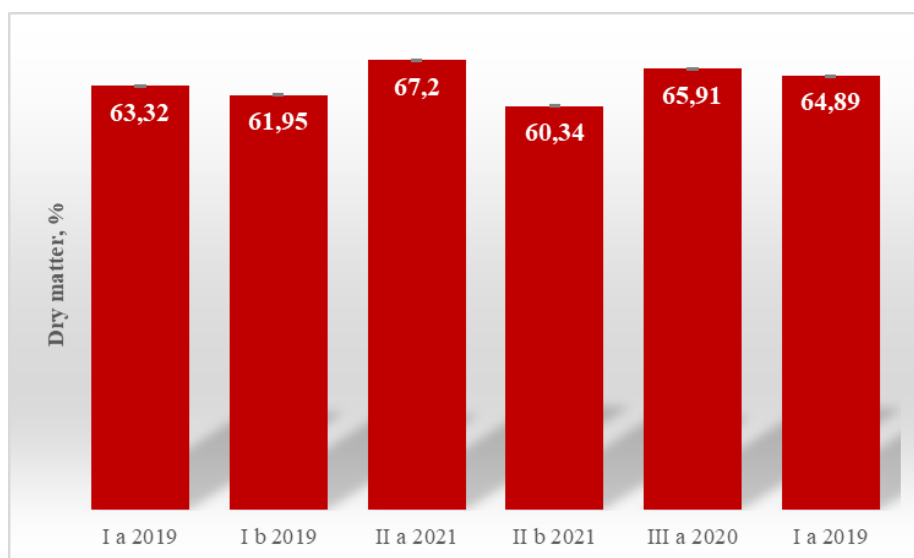


Fig. 3. Dry matter of compost samples

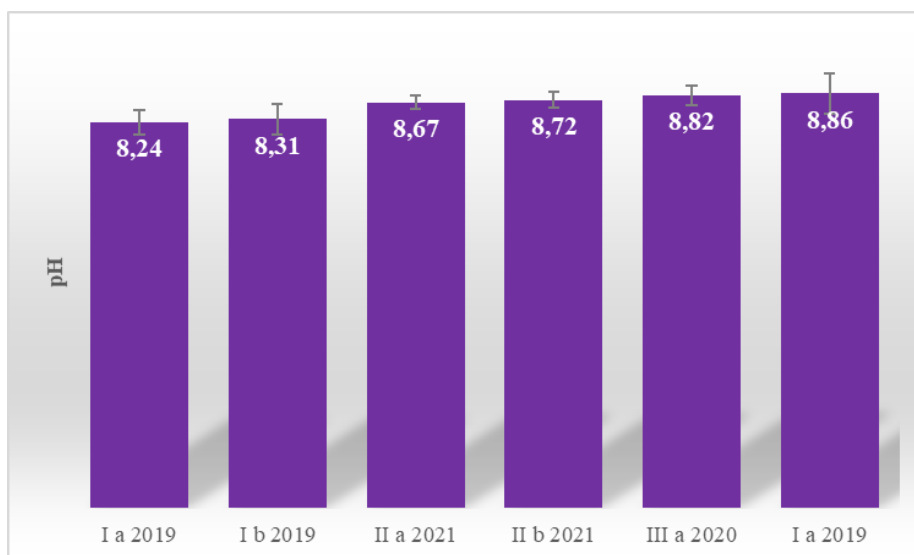


Fig. 4. pH variation of compost samples obtained in 3 different years

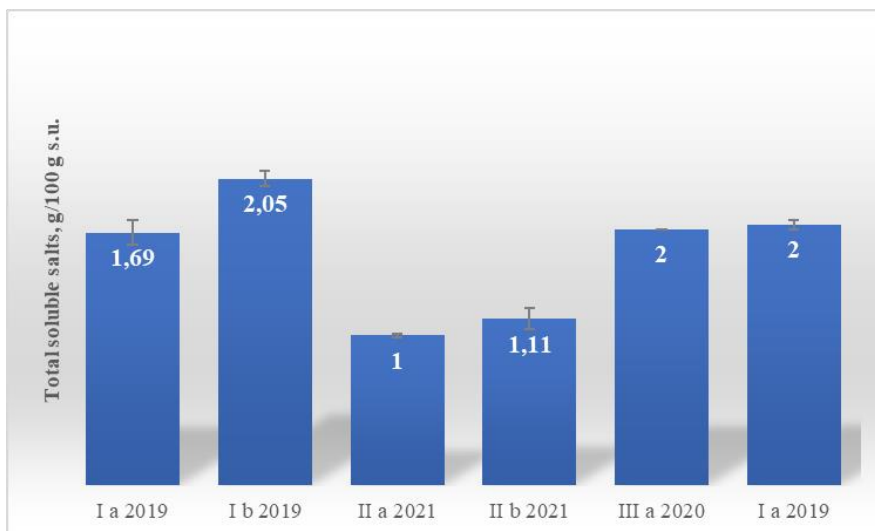


Fig. 5. Variation of total soluble salts in compost



Fig. 6. Variation of organic matter content in compost



Fig. 7. Variation of nitrate nitrogen content



Fig. 8. Variation of ammoniacal nitrogen content

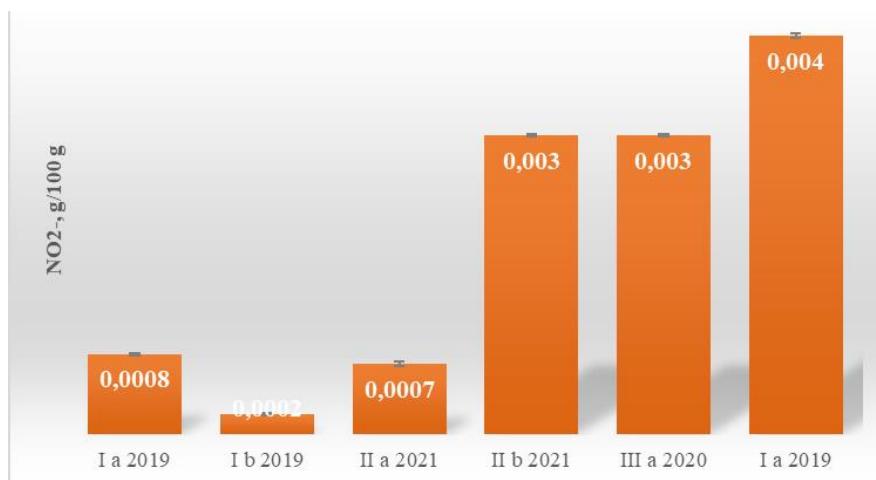


Fig. 9. Variation of nitrite content

3.2. The use of compost as a biofertilizer in the greenhouse for tomato culture

The compost was considered complete when the temperature in the composting mass had stabilized at a value close to that of the ambient environment and the oxygen concentration in the middle of the pile remained at values above 5% for several days. These measurements were made when the compost mass had a moisture content of no more than 50% and sufficient volume for the heating process not to occur. In order to be applied as a biofertilizer during the growing season the compost must be properly decomposed. Organic matter with a high C:N ratio competes with plant roots for accessible soil nitrogen. Microorganisms that mine carbon from organic matter have a higher affinity for nitrogen than plant roots. Testing of compost as a biofertilizer was

carried out under greenhouse conditions in an experimental tomato plot where it was found that organic matter and soil pH increased in relation to use rates. Compared to the control soil, beneficial influences were observed in the one supplemented with compost. Plants developed faster and stronger and with higher production because the compost supplemented the soil with nutrients and essential microelements necessary for plant growth. The speed of nutrient transfer has been reduced, the compost binds nutrients, ensuring that they are released and used over a longer period of time. Nutrient fixation reduces nutrient leaching to groundwater and surface water during rainfall and irrigation. Soil porosity was improved, microbiological activity is optimal in fertile soils. Microorganisms break down macromolecular organic substances and provide plants the necessary nutrients, but this phenomenon is increased in porous, aerated soils because the

biodegradation process is an aerobic process. The water retention capacity was improved, both by increasing soil porosity and by the capacity of compost to absorb water. The resistance of the soil to erosion was improved, by improving the physical characteristics of the soil and the faster growth of plants due to the accessibility of water and nutrients. The application of compost reduced the incidence of pathogens in plant contamination.

4. Conclusion

Composting is a biochemical process of mineralization of organic compounds, which under natural conditions occurs mainly in the soil. The need to compost waste under controlled conditions is dictated by the following considerations: environmental protection, conversion of biodegradable waste into biofertilizer-compost, used as a quality natural fertilizer, improve natural soil quality, increase productivity, plant health and also increases the quality of life and promote the principle of circular economy.

The studies presented in this paper lead to the following conclusions and perspectives: composting waste on the farm is a useful way to reduce the amount of vegetable waste and obtain a valuable biofertilizer under simple conditions. The compost samples analysed showed a high physicochemical quality. The application to tomato greenhouses, it has led to improved productivity and quality of crops and

soil. The use of compost offers environmentally friendly solutions with a long-term impact on the environment and quality of life.

References

- [1]. Igalavithana A. D., Kim K.-H., Jung J.-M., Heo H.-S., Kwon E. E., Tack F. M., Tsang D. C., Jeon Y. J., Ok Y. S., *Effect of biochars pyrolyzed in N₂ and CO₂, and feedstock on microbial community in metal (loid)s contaminated soils*, Environ. Int. 126, p. 791-801, 2019.
- [2]. ***, <https://www.icpa.ro>.
- [3]. ***, apmdj.anpm.ro.
- [4]. Dreghiciu C., *Materiale ecologice utilizate ca biofertilizatori și adsorbanti ai metalelor grele din apele uzate*, Rezumatul tezei de doctorat. Facultatea Design de Produs și Mediu, Universitatea Transilvania din Brașov, 2013.
- [5]. Rynk R., *et al.*, *On Farm Composting Handbook*, Northeast Regional Agricultural Engineering Service. Available from NRAES, Cooperative Extension, 152 Riley-Robb Hall, Ithaca, NY 14853-5701, (607), p. 255-7654, 1992.
- [6]. Waqas M., Nizami A., Aburiazaiza A., Barakat M., Ismail I., Rashid M., *Optimization of food waste compost with the use of biochar*, J. Environ. Manag., 216, p. 70-81, 2018.
- [7]. Legros J. P., Petruzzelli G., *The status of Mediterranean soils*, Int. Conf. Soil & Biowaste in Southern Europe, Rome, Italy, 2001.
- [8]. Amlinger F., Peyr S., Geszti J., Dreher P., Karlheinz W., Nortcliff S., *Beneficial Effects of Compost Application on Fertility and Productivity of Soils*, Literature Study Federal Ministry for Agriculture and Forestry, Environment and Water Management, Austria, 2007.
- [9]. Diacono M., Montemurro F., *Long-term effects of organic amendments on soil fertility A review*, Agron. Sustain. Dev., 30, p. 401-422, 2010.

MANUSCRISELE, CĂRȚILE ȘI REVISTELE PENTRU SCHIMB, PRECUM ȘI ORICE
CORESPONDENȚE SE VOR TRIMITE PE ADRESA:

MANUSCRIPTS, REVIEWS AND BOOKS FOR EXCHANGE COOPERATION,
AS WELL AS ANY CORRESPONDANCE WILL BE MAILED TO:

LES MANUSCRIPTS, LES REVUES ET LES LIVRES POUR L'ÉCHANGE, TOUT AUSSI
QUE LA CORRESPONDANCE SERONT ENVOYÉS À L'ADRESSE:

MANUSKRIPTEN, ZIETSCHRIFTEN UND BUCHER FÜR AUSTAUCH SOWIE DIE
KORRESPONDENZ SIND AN FOLGENDE ANSCHRIFT ZU SENDEN:

After the latest evaluation of the journals by the National Center for Science Policy and Scientometrics (**CENAPOSS**), in recognition of its quality and impact at national level, the journal will be included in the B⁺ category, 215 code (http://cncsis.gov.ro/userfiles/file/CENAPOSS/Bplus_2011.pdf).

The journal is already indexed in:

DOAJ: <https://doaj.org/>

SCIPIO-RO: <http://www.scipio.ro/web/182206>

EBSCO: <http://www.ebscohost.com/titleLists/a9h-journals.pdf>

Google Academic: <https://scholar.google.ro>

Index Copernicus: <https://journals.indexcopernicus.com>

Crossref: <https://search.crossref.org/>

The papers published in this journal can be viewed on the website:
<http://www.gup.ugal.ro/ugaljournals/index.php/mms>

Name and Address of Publisher:

Contact person: Prof. Dr. Eng. Elena MEREUȚĂ
Galati University Press - GUP
47 Domneasca St., 800008 - Galati, Romania
Phone: +40 336 130139
Fax: +40 236 461353
Email: gup@ugal.ro

Name and Address of Editor:

Ș. L. Dr. Eng. Marius BODOR
“Dunarea de Jos” University of Galati, Faculty of Engineering
111 Domneasca St., 800201 - Galati, Romania
Phone: +40 336 130208
Phone/Fax: +40 336 130283
Email: marius.bodor@ugal.ro

AFFILIATED WITH:

- **THE ROMANIAN SOCIETY FOR METALLURGY**
- **THE ROMANIAN SOCIETY FOR CHEMISTRY**
- **THE ROMANIAN SOCIETY FOR BIOMATERIALS**
- **THE ROMANIAN TECHNICAL FOUNDRY SOCIETY**
- **THE MATERIALS INFORMATION SOCIETY**
(ASM INTERNATIONAL)

**Edited under the care of
the FACULTY OF ENGINEERING**
Annual subscription (4 issues per year)

Fascicle DOI: <https://doi.org/10.35219/mms>

Volume DOI: <https://doi.org/10.35219/mms.2023.3>

Editing date: 15.09.2023

Number of issues: 200

Printed by Galati University Press (accredited by CNCSIS)
47 Domneasca Street, 800008, Galati, Romania